46th AIAA Aerospace Sciences Meeting and Exhibit
7 - 10 January 2008, Reno, Nevada

AIAA 2008-746

Numerical Simulations of Strong Shock and Disturbance Interactions Using High-Order Shock-Fitting Algorithms

Pradeep S. Rawat[1] and Xiaolin Zhong[2]
University of California, Los Angeles, CA, 90095

High order methods that can solve flows involving interactions of flow-disturbances with shock waves are critical for reliable numerical simulation of strong-shock and turbulence interaction problems. Such problems are not well understood due to limitations of numerical methods. For numerical simulation of compressible flows, shock capturing schemes have been the most popular choice. However, most of such methods are inherently dissipative and may incur numerical oscillations near the shock. Present paper focuses on developing and implementing new algorithms based on shock-fitting and front-tracking methodology which can solve the flow with high-order accuracy near as well as away from the shocks. The shock-fitting algorithm avoids dissipation and possible numerical oscillations incurred in shock-capturing methods by treating shocks sharply. We explore two ways for shock-fitting: conventional moving grid set-up and a new fixed grid set-up with front tracking. Conventionally, shock fitting is implemented on moving grid while shock forms a boundary of the computational domain. However, shock-fitted grid generation can be tedious for large and complex motions of the shock-front. Hence, we have also worked on developing a fixed grid set-up for shock-fitting method where shock is tracked using Lagrangian points and is free to move across underlying fixed grid. Using these shock-fitting algorithms we have solved one and two dimensional interactions of shock and vorticity/entropy disturbance waves and results have been found to be very satisfactory. We have also carried out a rate of convergence study to establish that, unlike shock-capturing schemes, the shock-fitting methods are high-order accurate near the shock. Although problems considered in this paper are relatively simple, the quality of results obtained from shock-fitting method provides good motivation to pursue it further for the problems of shock-turbulence interactions. In future, fixed grid shock-fitting methodology will be further developed with Immersed interface method of Zhong [1, 2] and more robust front-tracking algorithms so that more complex shock-turbulence interaction problems can be considered.

NOMENCLATURE

c= local speed of sound
e= total energy of fluid
M= Mach number
Pr = Prandtl number
q= heat flux vector
T= temperature
T_∞= sonic temperature
U_∞ = sonic velocity at lab conditions
x,y,z= Cartesian coordinates
γ = ratio of specific heats
$\bar{\tau}$ = viscous stress tensor
C_v = constant volume specific heat
J= Jacobian of grid transformation
p= pressure
P_0= stagnation pressure of inlet flow.
t = time
T_r= reference temperature
T_o= stagnation temperature
u,v,w = Cartesian velocity components
ρ= density of fluid
μ= dynamic viscosity

[1]Graduate Student, Mechanical and Aerospace Engineering Deptt. pradeep@seas.ucla.edu, Student Member, AIAA
[2]Professor, Mechanical and Aerospace Engineering Department, Associate Fellow, AIAA.

1 INTRODUCTION

Many important scientific and engineering applications involve complex interactions between turbulent flows and strong shocks. Such interactions are part of a number of explosive processes such as volcanic eruptions, detonations, shock wave lithotripsy to break up kidney stones, supernova explosion, as well as the implosion of a cryogenic fuel capsule for inertial confinement fusion (ICF). Numerical simulation of such complex problems warrants very high-order numerical methods. However, popular shock-capturing schemes are not very accurate in this regard as they use dissipation near the shock. Moreover, spurious numerical oscillations have also been observed when solving strong-shock and flow interaction problems with shock-capturing schemes [3]. In the present study, we investigate shock-fitting algorithms for shock and disturbance interaction studies. Problem of interaction of normal shock and disturbances is fundamental for better understanding of the aforementioned complex phenomena. To this end, shock-fitting methods developed in current effort can be very useful to find high-order solutions of some simple shock and turbulence interaction problems such as shown in Fig. 1. Various researchers have considered such shock and disturbance/turbulence interaction problems in past. A brief summary is presented in ensuing sections for previous works in the field, followed by the scope of current study.

1.1 Theoretical Studies

Theoretical studies in this field have been attempted mostly through linear interaction analysis (LIA) where small perturbations in flow are considered. Kovasznay [4] showed that for weak fluctuations of density, pressure, and entropy, the turbulent fluctuations about mean uniform flow can be decomposed into the vorticity, acoustic, and entropy modes. It was shown that for first order approximation, each of these modes evolve independently in the inviscid limit for mean uniform flow. However, in second order approximation of fluctuations, interaction of these modes is possible and one mode can be generated from interaction of other two modes [5].

Ribner [6-8] and Moore [9] were among the earliest workers to consider theoretically the passing of a turbulent field through a shock wave. Ribner [6] analyzed interaction of a plane sinusoidal disturbance in velocity (shear wave) passing through a shock as a boundary value problem. In his analysis the shock was kept steady by solving the equations in a moving reference frame. It was found that initial shear wave is amplified and refracted by the shock due to the changes in thermodynamic properties and therefore emerges at a different angle from the incident. He later generalized this result from single wave to obtain shock-interaction effects of a completely turbulent velocity field [7] and obtained significant turbulent amplification due to shock turbulence interaction. The results were further extended [8] to provide the flux of acoustic energy emanating from unit area on the downstream of the shock. Moore [9] performed unsteady analysis of interaction of obliquely traveling weak plane disturbances of arbitrary profile with a plane normal shock. Unlike Ribner's analysis, unsteady shock was considered for linear analysis the interaction of sound and vorticity waves with an unsteady shock. It was found that amplification of disturbances depends on impingement angle and Mach number of the shock. Kerrebrock [10] considered modifications of random small fluctuations of pressure, entropy and vorticity in passing through shock or flame. It was found that all modes of disturbances are generated in the downstream flow if any of the modes is present in the upstream flow. McKenzie and Westphal [11] derived formulas for amplification and Snell's Laws for refraction and

reflection of acoustic, vorticity and entropy waves interacting with shock and applied the results to the amplification of small disturbances in the solar wind on a passage through the bow shock of earth. More recent theoretical studies of shock and turbulence interaction are by Goldstein [12], Lee et al. [13-15], Mahesh et al. [16-18] and Fabre et al. [19, 20]. It was found in these studies that different components of the turbulent kinetic energy, as well as root mean square values of the fluctuating pressure, temperature and density are amplified across the shocks. Despite several assumptions, Linear Interaction Analysis (LIA) provides accurate description of the essential characteristics of the interaction.

1.2 Numerical Studies

Since the early 80s, various attempts have been made towards numerical simulation of shock and disturbance/turbulence interaction. Initial efforts in this regard considered interaction of shock with simple waves. In 1981, Pao and Salas [21] fitted the shock at inflow boundary and solved Euler equation with finite difference discretization for study of shock/vortex interaction. Shock fitting computations with pseudo-spectral (Zang et. al [22]) and spectral techniques (Hussaini et al [23, 24]) were later used to treat the problems in which a single vortex, a vortex sheet, an entropy spot or acoustic wave interacts with the shock. The results obtained from these numerical efforts confirmed the linear theory in the regime of weak shocks. With the advent of essentially non-oscillatory (ENO) and related schemes, shock-capturing methods gained popularity for simulations of compressible flows. A number of new schemes for compressible flows has since been tested for interaction of shock with small disturbances against the results obtained from linear theory [24-26]. Although limited to low Mach numbers, these studies mostly confirm the LIA results.

The numerical studies of fully turbulent field interacting with shocks are more recent. For the simulation of the turbulent field DNS methods and large eddy simulations (LES) have been used. However these different types of methods give different results when interaction with shock is considered [27]. Most of the recent direct numerical simulation (DNS) studies have been on various aspects of interaction of a normal shock with freestream turbulence for relatively weak shock of small Mach numbers. For example, Mahesh et al. [16, 18] did extensive direct numerical simulation (DNS) study of the interaction of a normal shock with an isotropic turbulence. The mean shock Mach numbers were in the range of 1.29 to 1.8. They found that the upstream correlation between the vorticity and entropy fluctuations has strong influence on the evolution of the turbulence across the shock. They also used linear analysis to analyze the simulation results. Other shock/turbulence interaction studies have been conducted by the same group of workers [13, 14]. Lee et al. [14] investigated the effect of Mach number on isotropic vertical turbulence interacting with a shock wave. The range of Mach numbers was in the range from 1.5 to 3.0. A shock-capturing scheme was developed to accurately simulate the unsteady interaction of turbulence with shock waves. It was found that turbulence kinetic energy is amplified across the shock wave, and this amplification tends to saturate beyond Mach 3. Hannapel et al. [28] computed interaction of a Mach 2 shock with a third order in space shock-capturing scheme based on the essentially non-oscillatory ENO algorithm of Harten together with an approximate Riemann solver. Jamme et al. [29] carried out a Direct Numerical Simulation (DNS) to study the interaction between normal shock waves of moderate strength (Mach 1.2 and Mach 1.5) and isotropic turbulence. Adams and Shariff [30, 31] proposed a class of upwind-biased finite-difference schemes with a compact stencil for shock/turbulence

interaction simulation. They used this nonconservative upwind scheme in smooth region while a shock-capturing ENO scheme was turned on around discontinuities. This idea of hybrid formulation was improved by Pirozzoli [32] who used similar hybrid formulation for a compact weighted essentially non-oscillatory (WENO) scheme with conservative formulation for simulation of shock turbulence interaction. Ducros et al. [33] developed larger-eddy simulation(LES) on the shock/turbulence interaction by using a second-order finite volume scheme. The method was then used to simulate the interaction of a Mach 1.2 shock with homogeneous turbulence.

Yee et al. [34] proposed characteristic-type filters, which add the dissipative part of traditional shock capture schemes to non-dissipative central based schemes in order to damp out numerical instabilities. Due to this feature, characteristic filters are very suitable to incorporate into existing LES codes based on high-order methods, and they allow the codes to have shock capturing capability. This scheme was used by Sjogreen and Yee [35] for shock disturbance interaction. Recently, Cook and Cabot [36, 37] developed artificial viscosity formulations for shock-turbulence simulations. It functions as an effective subgrid-scale model for both high and low Mach number flows. The model employs a bulk viscosity for treating shocks and a shear viscosity for treating turbulence and has been used for the basic shock disturbance interaction.

It is observed that most of the studies in field of shock-turbulence interaction have considered weak shocks only. Recently, more efforts have been directed towards investigating turbulent flows with stronger shocks which is relevant for a lot of high-speed compressible flows. Main issue with shock-capturing schemes is spurious numerical oscillations around the shock and loss of accuracy with dissipation needed to suppress these oscillations. Moreover, with stronger shocks, shock-thickness reduces which requires a finer resolution with shock-capturing schemes. Shock-fitting method offers a good alternative for strong shocks with simple geometries as shock is considered a sharp discontinuity. As mentioned before, one of the earliest numerical methods considered for shock-disturbance interactions were based on shock-fitting methodology. Shock-fitting methods have also been very successful for high-order simulations for freestream disturbances interacting with shock on blunt body [38-41] . Recently, Sesterhenn et al. [42] revisited shock-fitting schemes and applied them for solving Navier-Stokes equations in non-conservative form for problem of interaction of Mach 3 shock with isotropic turbulence with encouraging results. Shock-fitting considers the shock as a sharp discontinuity and is well equipped to consider even stronger shocks without any need for grid refinements. However, grid generation for conventional shock-fitting can become tedious if there are large and complex changes in shock-geometry. Hence, to take advantage of high-order accuracy of shock-fitting algorithms for more general problems, there is need for implementation of a front-tracking based shock-fitting methodology where shock can move across the fixed grids.

1.3 Motivation and Scope of Current Study

A study of the literature in the field of shock interactions with disturbances and turbulence shows that these complex configurations are part of a number of important phenomena including supernova explosions and inertial confinement fusion. However, the current scientific understanding of shock-turbulence interactions in complex configurations and the ability to reliably predict these strongly nonlinear flows remains limited. Most of the popular methods for solving compressible flow involve shock-capturing algorithms for treatment of

shock. However, it has been observed that even high-order shock capturing methods give low accuracy at the shock [43] and might lead to spurious oscillations [3]. Many shock capturing methods introduce some dissipation to avoid spurious oscillations which, however, is not accurate enough for simulation of turbulent flow. On the other hand, conventional high-order methods generally used for DNS studies have numerical problems due to strong gradients around shock. Due to such problems, DNS of shock and isotropic turbulence interaction has not been possible for stronger than Mach 3 shocks due to limitations of computational resources for the used shock capturing algorithms.

In present study, we develop and use shock-fitting algorithms along with high order schemes to gain knowledge about nonlinear phenomena involving interaction of strong shocks and flow disturbances. Shock fitting algorithms treat the shock-interface sharply without any dissipation hence they are compatible with low dissipation schemes used for DNS of turbulent flow. Shock/interface fitting methods are ideally suited for the cases where there is a clearly demarcated interface such as observed in the problems involving disturbances coming towards the normal shock. Some of canonical problems in one and two dimensional space have been considered in this paper and results obtained point to the superiority of the shock-fitting methods for such problems.

Conventionally, shock is treated as boundary in shock-fitting methods and grids follow the shock during the computations. This, however, might not be feasible if shape of the shock becomes complex or there are large movements in shock. For such situations, it is more appropriate to extend high-order shock-fitting idea to use it with fixed grids where shock moves independent of grids. To this end, we are developing a fixed grid shock-fitting solver. This solver intends to solve the flow on a fixed Cartesian or curvilinear grid while shock is tracked using a front tracking algorithm (e.g. [44]) . Current implementation of the code use one-sided finite differences near the shock points and works well for the simple shock-disturbance interaction problems. We intend to work on the fixed grid shock-fitting method further and include our new high-order immersed interface method [1, 2] with a robust front tracking algorithm. Such high-order implementation, if successful, will be very helpful in solving other multi-phase problems as well.

Thus main thrust of current study includes (a) asses the efficiency and results of conventional shock-fitting algorithm for some canonical problems (b) implementing shock-fitting algorithm with a fixed grid solver and (c) ensure high order accuracy by carrying out order of convergence analysis.

In remaining part of this paper we briefly present the governing equations and numerical method followed by solutions for the cases of 1-D and 2-D disturbances interacting with shock.

2 GOVERNING EQUATIONS

The governing equations are compressible Navier-Stokes equations which are given as follows:

$$\frac{\partial \rho}{\partial t} + \nabla.(\rho \mathbf{u}) = 0 \qquad (1)$$

$$\rho\left(\frac{\partial \mathbf{u}}{\partial t}+\mathbf{u}\cdot\nabla\mathbf{u}\right)=-\nabla p+\nabla\cdot\overline{\overline{\tau}} \tag{2}$$

$$\frac{\partial e}{\partial t}+\nabla\cdot(e\mathbf{u})=-\nabla\cdot(p\mathbf{u})+\nabla\cdot(\mathbf{u}\cdot\overline{\overline{\tau}})-\nabla\cdot\mathbf{q} \tag{3}$$

where $e=\frac{p}{(\gamma-1)}+\frac{1}{2}\rho U^2$, is the internal energy plus the kinetic energy of the fluid. The viscous stress and the heat flux are given by the usual constitutive equations in Newtonian fluid as follows

$$\tau_{ij}=\mu\left(\frac{\partial u_i}{\partial x_j}+\frac{\partial u_j}{\partial x_i}\right)-\frac{2}{3}\mu\frac{\partial u_k}{\partial x_k}\delta_{ij} \tag{4}$$

$$q_i=-k\frac{\partial T}{\partial x_i} \tag{5}$$

where μ is the viscosity coefficient determined by the Sutherland law,

$$\mu=\mu_r\left(\frac{T}{T_r}\right)^{\frac{3}{2}}\frac{T_r+T_s}{T+T_s} \tag{6}$$

where T_r = 288K, T_s = 110K, and μ_r = 0.17894 × 10^{-4} kg/m/s for air. The thermal conductivity k is computed from the Prandtl number, which is assumed constant and it takes the value of 0.72 in this paper.

3 NUMERICAL METHOD: CONVENTIONAL HIGH-ORDER SHOCK-FITTING

For conventional moving-grid shock-fitting approach, shock forms a boundary of the computational domain and fifth-order shock-fitting method of Zhong [45] is used for solving the flow between shock and exit boundary (Fig. 1). The flow variables just behind the shock are determined by Rankine-Hugoniot relations across the main shock and a characteristic compatibility relation from behind the shock. The velocity and location of the shock are solved as part of the solutions and grid is modified to follow motions of the shock. In the interior, solution of conservative compressible Navier-Stokes equations is carried out using the numerical method described in this section.

In numerical simulation, the compressible Navier-Stokes equations (2) to (4) are written in the following conservative form,

$$\frac{\partial U}{\partial t}+\frac{\partial E}{\partial x}+\frac{\partial F}{\partial y}+\frac{\partial G}{\partial z}+\frac{\partial E_v}{\partial x}+\frac{\partial F_v}{\partial y}+\frac{\partial G_v}{\partial z}=0 \tag{7}$$

where U is the solution vector given by

$$U=\{\rho,\rho u,\rho v,\rho w,e\} \tag{8}$$

E, F, G are the inviscid flux terms, and E_v, F_v, G_v are the viscous terms. They are written as follows

$$E=\begin{Bmatrix}\rho u\\ \rho u^2+p\\ \rho uv\\ \rho uw\\ (e+p)u\end{Bmatrix} \tag{9}$$

$$F=\begin{Bmatrix}\rho v\\ \rho vu\\ \rho v^2+p\\ \rho vw\\ (e+p)v\end{Bmatrix} \tag{10}$$

$$G=\begin{Bmatrix}\rho w\\ \rho wu\\ \rho wv\\ \rho w^2+p\\ (e+p)w\end{Bmatrix} \tag{11}$$

$$E_v=\begin{Bmatrix}0\\ \tau_{xx}\\ \tau_{yx}\\ \tau_{zx}\\ u\tau_{xx}+v\tau_{yx}+w\tau_{zx}-q_x\end{Bmatrix} \tag{12}$$

$$F_v = \begin{Bmatrix} 0 \\ \tau_{xy} \\ \tau_{yy} \\ \tau_{zy} \\ u\tau_{xy} + v\tau_{yy} + w\tau_{zy} - q_y \end{Bmatrix} \tag{13}$$

$$G_v = \begin{Bmatrix} 0 \\ \tau_{xz} \\ \tau_{yz} \\ \tau_{zz} \\ u\tau_{xz} + v\tau_{yz} + w\tau_{zz} - q_z \end{Bmatrix} \tag{14}$$

In the conservative equation (7), the inviscid fluxes and the viscous fluxes have the same forms as those of the Navier-Stokes equations. Before discretizing the governing equations by a finite difference method, equation (7) in the physical domain is transformed to the shock and boundary fitted computational domain by the following transformation relations,

$$\begin{cases} \xi = \xi(x, y, z) \\ \eta = \eta(x, y, z) \\ \varsigma = \varsigma(x, y, z) \\ \tau = t \end{cases} \Leftrightarrow \begin{cases} x = x(\xi, \eta, \varsigma, \tau) \\ y = y(\xi, \eta, \varsigma, \tau) \\ z = z(\xi, \eta, \varsigma, \tau) \\ t = \tau \end{cases} \tag{15}$$

and the transformed governing equation in the computational domain is expressed as follows

$$\frac{1}{J}\frac{\partial U}{\partial \tau} + \frac{\partial E'}{\partial \xi} + \frac{\partial F'}{\partial \eta} + \frac{\partial G'}{\partial \varsigma} + \frac{\partial E'_v}{\partial \xi} + \frac{\partial F'_v}{\partial \eta} + \frac{\partial G'_v}{\partial \varsigma} + U\frac{\partial\left(\frac{1}{J}\right)}{\partial \tau} = 0 \tag{16}$$

An explicit finite difference scheme is used for spatial discretization of the governing equation (18), the inviscid flux terms are discretized by a fifth-order upwind scheme, and the viscous flux terms are discretized by a sixth-order central scheme. For the inviscid flux vectors, the flux Jacobians contain both positive and negative eigenvalues. A simple local Lax-Friedrichs scheme is used to split vectors into negative and positive wave fields. For example, the flux term F′ in Eq (18) can be split into two terms of pure positive and negative eigenvalues as follows

$$F' = F'_+ + F'_- \tag{17}$$

where $F'_+ = \frac{1}{2}(F' + \lambda U)$ and $F'_+ = \frac{1}{2}(F' - \lambda U)$ and λ is chosen to be larger than the local maximum eigenvalue of F′.

$$\lambda = \frac{|\nabla \eta|}{J}\left(\sqrt{(\varepsilon c)^2 + u'^2} + c\right) \tag{18}$$

where

$$u' = \frac{\eta_x u + \eta_y v + \eta_z w + \eta_t}{|\nabla \eta|} \tag{19}$$

The parameter ε is a small positive constant added to adjust the smoothness of the splitting. The fluxes F'_+ and F'_- contain only positive and negative eigenvalues respectively. Therefore, in the spatial discretization of Eq. (7), the derivative of the flux F is split into two terms

$$\frac{\partial F'}{\partial \eta} = \frac{\partial F'_+}{\partial \eta} + \frac{\partial F'_-}{\partial \eta} \tag{20}$$

where the first term on the right hand side is discretized by the upwind scheme and the second term by the downwind scheme.

The fifth-order explicit scheme utilizes a 7-point stencil and has an adjustable parameter α as follows

$$u'_i = \frac{1}{hb_i}\sum_{k=-3}^{3} a_{i+k}u_{i+k} - \frac{\alpha}{6!b_i}h^5\left(\frac{\partial^6 u}{\partial x^6}\right)_i + \ldots \tag{21}$$

where $\alpha_{i\pm3} = \pm 1 + \frac{1}{12}\alpha,\ \alpha_{i\pm2} = \mp 9 - \frac{1}{2}\alpha,\ \alpha_{i\pm1} = \pm 45 + \frac{5}{4}\alpha,\ \alpha_i = -\frac{5}{3}\alpha$ and $b_i = 60$. The scheme is upwind when $\alpha < 0$ and downwind when $\alpha > 0$. It becomes a 6-order central scheme when $\alpha = 0$ which is used for discretizing viscous terms.

4 NEW FRONT-TRACKING BASED FIXED-GRID HIGH-ORDER SHOCK-FITTING METHOD

Conventional shock-fitting methodology, as described in previous sections, assumes the shock to be the boundary of the domain and flow is solved on moving grids. However, this approach becomes very difficult to apply for a problem where shock geometry becomes complex or the shock performs large motions. Hence, it is useful to develop a methodology that can implement ideas of shock-fitting algorithm on fixed grids. We have explored a fixed grid shock-fitting method where shock is treated as an interface and can move across the fixed grid points. Thus the method is along the lines of fixed grid Cartesian grid methods like Immersed Boundary Method (IBM), Immersed Interface Method (IIM), Ghost fluid methods etc. coupled with methods to track the front (shock). The methodology is presented here in brief for two dimensional problems.

4.1 Finite difference scheme

Similar to the conventional shock-fitting, governing equations are solved in the conservation form of equations and physical domain is transformed to computational domain and

flux splitting is performed for application of upwind finite-difference schemes. Thus i.e. Eqs. (1) -(20) are still applicable in this formulation except fixed grids used making Jacobian of grid-transformation constant. The 5th order upwind method given by (21) can be used on the points where finite-difference stencil does not cross the front. However, special treatment is needed for the "irregular" points where the stencil requires points on both sides of the shock. An example of irregular points on a grid line in X-direction is shown as the highlighted points shown in Fig.2 for 7 point 5th order scheme. Similar irregular grid points can also be found for Y-direction grid line.

To avoid crossing the shock-front with our stencils we use one-sided finite differencing on irregular points. Interface point is included in the stencil along with interior points and we use one sided Lagrange interpolation to find derivative of any variable u at point as follows:

$$\left[\frac{\partial u}{\partial x}\right]_{x=x_j} = \sum_{k=-n+1}^{0} l_k'(x_j)u_{i+k} + l_\Gamma'(x_j)u_\Gamma \tag{22}$$

where subscript Γ indicates interface point, x_i is the nearest point to the interface that is taken in the one sided difference stencil and Lagrane coefficients l_k's and l_Γ are given as

$$\begin{aligned} l_k(x) &= \frac{\sum_{p=0,p\neq k}^{-n+1}(x-x_{i+p})}{\sum_{p=0,p\neq k}^{-n+1}(x_{i+k}-x_{i+p})}\left(\frac{(x-x_\Gamma)}{(x_{i+k}-x_\Gamma)}\right) \\ l_\Gamma(x) &= \frac{\sum_{p=0}^{-n+1}(x-x_{i+p})}{\sum_{p=0}^{-n+1}(x_\Gamma-x_{i+p})} \end{aligned} \tag{23}$$

It should be noted that when using one-sided derivatives there might be issues with stability of the method if one of the grid-point is too close to the interface. Hence for one-sided approximation (using Lagrange interpolations), we should have two different cases

(a) When marker point and interface have reasonable separation (as shown in Fig. 3(a) then include in the stencil, the marker point as well as the closest point and store all the coefficients (as shown in the figure 3(a)).
(b) When marker point and one of the interface point are too close, we will include the marker point but leave out the closest grid point and include a grid point on other end instead (as shown in Fig. 3(b)).

We use one-sided finite difference scheme to avoid finite difference stencils crossing the shock-front. However, if appropriate jump conditions are known at the shock-front, one can use schemes like Immersed interface methods (IIM) that find the finite differences at irregular grid points using regular stencil and correction terms based on jump conditions. Such methods allow flow of information across the shocks and can be more accurate as accurate jump conditions are enforced. Recently, Zhong [1, 2] developed a new immersed interface algorithm that requires

jumps only in values of flow variables and their first derivatives while showing arbitrarily high-order accuracy. Since upto first order jump conditions can be derived from physics of the problem, this method is more suitable for high-order computations of real problems than other IIM schemes which need higher order derivatives of flow variables to obtain higher order of accuracy. Hence, we intend to explore new IIM method of Zhong [1, 2] in future for finite differencing in the computational domain.

4.2 Representation of the front

In our methodology, the shock-front is assumed to be sharp and is represented using Lagrangian marker points. The marker points connect segments of 5^{th} order polynomial curves. or convenience in taking finite differences across the shock front, intersection points of the front with the grid lines are chosen as marker points. Figure 4 shows typical marker points (S_i, S_{i+1} etc.) for a shock-front moving across a two-dimensional grid. These marker points are stored in a sequenced list. The order in list indicates the immediate neighboring markers of a marker as shown in the Fig. 4. The notation used here is such that as we move along the markers by incrementing in this sequenced list, the low pressure side of the shock should be on the left. With each marker point, information regarding geometry of the front, flow properties corresponding to the marker points and relation of marker point with the fixed grid is also needed to be saved. Some important points about treatment of front are as follows:

Shock geometry:

With each marker point, coordinates of the marker points is computed and saved. A critical part of information regarding shock-geometry for shock-fitting method is shock shape, specifically shock normal and shock tangents which are obtained using the coordinates. We use following parametric representation for the marker points to obtain shock normal and shock tangents:

$$\begin{aligned} x &= x(s) \\ y &= y(s) \end{aligned} \tag{24}$$

where s represents the arc-length on the interface. Arc-length is chosen as the parameter to represent the surface since value of arc-length monotonically increases along the surface and each value of arc-length coordinate correspond to a unique point on the interface. Moreover, arc-length represents the value of body-fitted coordinate in the tangential direction which can be readily used to obtain tangential derivatives of various flow variables where needed. Using arc-length as parameter we use following definition for normal and tangent in 2-D.

$$n_x = \frac{\dfrac{\partial y}{\partial s}}{\left[\left(\dfrac{\partial x}{\partial s}\right)^2 + \left(\dfrac{\partial y}{\partial s}\right)^2\right]^{\frac{1}{2}}}, \quad n_y = \frac{-\dfrac{\partial x}{\partial s}}{\left[\left(\dfrac{\partial x}{\partial s}\right)^2 + \left(\dfrac{\partial y}{\partial s}\right)^2\right]^{\frac{1}{2}}},$$

$$\tau_{1x} = \frac{\dfrac{\partial x}{\partial s}}{\left[\left(\dfrac{\partial x}{\partial s}\right)^2 + \left(\dfrac{\partial y}{\partial s}\right)^2\right]^{\frac{1}{2}}}, \quad \tau_{1y} = \frac{\dfrac{\partial y}{\partial s}}{\left[\left(\dfrac{\partial x}{\partial s}\right)^2 + \left(\dfrac{\partial y}{\partial s}\right)^2\right]^{\frac{1}{2}}}, \tag{25}$$

This way of taking normal ensures that normal goes from high-pressure side towards low-pressure side. Thus using the direction of normal at any marker point we are able to determine orientation of high pressure side and low pressure side with respect to the given marker point. It should be noted, however, that arc-length is not directly known from the coordinate points. To obtain arclength and values of normal and tangents, we use an iterative procedure, where initial value of arclength is approximated as summed distance between the marker points. Using this approximate value as parameter we find coefficients of 5^{th} order polynomial segments and corresponding values of corrected arc length. The process is repeated till the values of arc-length are sufficiently converged.

Communication between the front and the grid

It can be observed that for two dimensional grid, there are two types of marker points: those at the intersection with Y=const line (ξ-grid line) and those at the intersection with X=const (η -grid line). Since each marker point is an intersection point, relation between grid and marker point is established by storing type of intersection point (intersecting with ξ-line or η -line) and indices for intersecting grid-line for each marker point. Indices of irregular grid points associated with marker points are also stored with each marker for efficient implementation of one-sided finite difference. Moreover, at each grid point, an indicator value is saved to associate the grid point with high pressure or low pressure side as appropriate. Shock velocity is obtained using the same shock fitting methodology as used for conventional shock-fitting with appropriate interpolations. Based on the shock velocity, marker points are moved to new locations and shock geometry and its relation with the grid is updated after each time step.

5 RESULTS: SHU-OSHER PROBLEM

For shock and disturbance interaction problems, validation of codes can be performed by comparing against standard results for relatively simple cases of one-dimensional and two-dimensional interactions of shock and disturbances. We have computed one-dimensional interaction of finite entropy wave and shock and compared it with available results from literature as presented in this section.

Shu-Osher problem, proposed by Shu and Osher in 1989 [46], presents a one-dimensional model of shock and turbulence interaction. The problem involves finite density variations (entropy disturbances) interacting with a moving normal shock for one dimensional inviscid configurations. The problem has strong nonlinear and fine scale features along with smooth regions. Hence, it has become a standard test case for shock capturing schemes (e.g. Visbal et al. [47] and Pirozzoli et al. [32]). Initial conditions of the problem are defined as follows:

At $t = 0$ for $x \le -4$ we have

$$\begin{aligned} \rho &= (\gamma+1)M^2 \big/ \left[(\gamma-1)M^2+2\right] \\ u &= 2\gamma^{1/2}\left(M^2-1\right)\big/\left[(\gamma+1)M\right] \\ p &= 1+2\gamma\left(M^2-1\right)\big/(\gamma+1) \end{aligned} \tag{26}$$

while for $x > -4$, we have

$$\begin{aligned} \rho &= 1.0 + \varepsilon \sin 5x \\ u &= 0.0 \\ p &= 1.0 \end{aligned} \tag{27}$$

where ρ , γ , u , M and p represent density, ratio of specific heats for the gas, velocity, Mach number and pressure respectively.

If $\varepsilon = 0.0$, we have a pure shock located at $x = -4$ at $t = 0$ and moving towards right with a constant velocity. If ε is small the problem remains linear and comparisons can be made with the results of Westphall and Mckenzie [11]. Validation of codes can be performed for capturing nonlinear phenomena by using a significantly large value of disturbance amplitude. This problem was solved by Shu and Osher for $M = 3.0$, $\gamma = 1.4$ and $\varepsilon = 0.2$ until $t = 1.8$. Since there is no analytic solution available for the non-linear problem, general practice for validation of shock capturing codes is to compute the problem with the parameters used by Shu and Osher and compare the result against a very fine grid solution. It should be noted, however, that strong nonlinearities in the problem can lead to spurious oscillations in shock capturing solutions even for fine grids.

5.1 Conventional shock-fitting with moving grids

We solved the Euler equations (Eq.(7) with zero viscosity) with the initial conditions given in Eqs.(26) and (27) using our two-dimensional fifth-order upwind method with shock-fitted moving grids using RK-3 time integration. The problem is computed in a reference frame moving with the steady state shock velocity so as to minimize the motion of shock for better shock fitting computations. It should be noted that flow upstream of the shock is supersonic relative to it; hence no effects of interaction will propagate upstream in shock reference frame. Thus, only the flow downstream of the shock constitutes region of interest. Therefore, with the conventional shock-fitted grids, it is viable to use the region bounded between the shock and the downstream boundary as computational domain for efficient shock-fitting computations as

shown in Fig. 5(a). Initial flow conditions are also shown in Fig. 5(a) which indicate use of a moving reference frame by our algorithm. The flow properties at streamwise boundaries remain unchanged throughout the solution procedure. Since we solve this one-dimensional problem in two-dimensional setting, we use periodic conditions at lateral boundaries. The initial density profile for the problem is shown in Fig. 5(b). Figure 5(c) shows the solution at non-dimensional time, $t = 1.8$. It can be seen from the figure that the density-disturbance amplifies after passing through the shock and causes nonlinear waves downstream. An enlarged view of the density variation downstream of the shock is shown in Fig. 6. As the shock propagates into the varying density field, an oscillatory solution develops behind the shock. A contact discontinuity develops in the middle of the flow downstream of the shock separating region immediately behind the shock from the small shocklets further downstream. Due to presence of small discontinuities behind the main-shock we need to use fourth-order artificial dissipation while computing the flow with very fine grids. Figures 5(c) and 6 also compare our results with those results obtained by Visbal et al.[47]. They used a hybrid scheme, having a five-point 6^{th} order compact spatial scheme with 10^{th} order spatial filter coupled with ROE scheme, to obtain the solution of Shu-Osher problem. They treated a very fine grid solution as the exact solution to investigate accuracy of results on coarser grids (See Fig. 6 of Ref. [47]). This reference solution is compared with fine-grid results obtained from our shock-fitting algorithm in Fig. 6. It can be seen that fine-grid results from two computations agree well in the region of interest. It can be noted, however, that the shock-fitting algorithm shows more prominent jump in density across the shock which can be attributed to shock not aligning with any grid point in shock capturing scheme.

5.2 Front-tracking based fixed-grid adaptation of shock-fitting

Fixed grid shock-fitting method, as described in section 4, can handle the large movements of the shock-front while keeping the grid-spacing constant. Hence, the problem defined by Eqs.(26) and (27) can be solved in the lab reference frame i.e. a Mach 3 shock moving into a still fluid having a spatially sinusoidal perturbation in the density. In this method, flow is solved upstream as well as downstream of the surface. In streamwise direction, unchanged boundary conditions are used at both ends while in lateral direction periodic conditions are used. Since problem is essentially same as the moving grid case, initial conditions shown in Fig. 5(b) are still valid. Motion of shock is tracked using marker points that can move across underlying fixed grid. Initial location of the marker points in our 2-D computational setting is shown in Fig. 7(a). The solution obtained after t=1.8 using the fixed grid method is compared to that obtained from the moving grid set-up in Fig 7(b), 7(c) and 7(d) for a coarse grid (grid spacing $dx = 0.05$). It is observed that the solution from the new fixed-grid shock-fitting method matches well to that obtained from the conventional moving grid set-up and small discontinuities in the post-shock flows are observed. With the coarse grids used for Fig. 7, the solution is stable without artificial dissipation but small wiggles are observed in flow-profiles in the region where discontinuities become strong in post-shock flow. These numerical wiggles also cause small differences between fixed-grid and moving-grid results around the point where expansion fan develops downstream of the flow (Fig. 7(b)). Accuracy and convergence of the front tracking based fixed-grid shock-fitting method is again assessed later in section 7.

5.3 Analysis of results

Since analytical results are not available for the Shu-Osher problem, we use a very fine grid solution with $N = 3200$ grid-points (on domain length of non-dimensional length 10 i.e grid

spacing, $dx = 3.125 \times 10^{-3}$) as reference to study quality of the solutions obtained from coarser grids. As already shown in section 5.1, this fine grid solution matches well to reference solutions used in literature. A comparison of density profiles obtained with various set of grids is shown in Fig. 8. It can be noted that with the coarsest grid considered ($N = 200$, $dx = 0.05$), the solution shows dissipation away from the main shock especially around the contact discontinuity. However, around the main fitted shock the solution shows very good agreement with the reference values even for the coarse ($N = 200$) grid. It should be appreciated that main shock represents the strongest nonlinearity in the solution. Hence, shock capturing schemes are expected to be most dissipative around main shock. On the other hand, shock-fitting code seems give accurate results around fitted shock even for a coarse grid which shows that a remarkable efficiency can be obtained from shock-fitting codes. As grid spacing is reduced to a half of the coarsest grid case, the solution greatly improves even in the regions away from fitted shock. It shows that, apart from the main shock, which is fitted, the weak discontinuities are effectively captured by our shock-fitting algorithm since we solve conservation form of Euler equations.

Incident density perturbations cause oscillations in the velocity behind the shock, even in absence of the velocity perturbations in upstream flow. The velocity perturbations at $t = 1.8$ are compared in Fig. 9 for solutions obtained at various grid-spacings. It can be noticed that the velocity perturbations travel behind the shock without significant changes in waveform while density values may encounter sharp changes which confirms presence of a contact discontinuity downstream of the shock. These oscillations in velocity steepen further downstream of the main shock forming small shocklets. Since discontinuities in velocity profiles are not as strong as those observed in density profiles, the coarse grid ($N = 200$) solution in Fig. 9 shows better agreement with the reference solution. However, significant errors are observed around the shocklets for coarse grid ($N = 200$) which reduce significantly with reduction in grid-spacing. Similar results are observed for profiles of other variables as well. A good estimate of the accuracy of results can be made by considering entropy solutions behind the shock. Nondimensional entropy of the fluid at pressure, p and density (ρ) can be defined as follows:

$$\frac{\Delta s}{C_p} = \frac{\ln p}{\gamma} - \ln \rho \tag{28}$$

where C_p is isobaric specific heat of the fluid. Thus, incoming density perturbations correspond to a 1-D entropy wave and leads to an entropy wave of a different amplitude and wavelength downstream of the shock. Figure 10 shows computed oscillations in nondimensionalized entropy for various grid resolutions. Finest grid solution, corresponding to $N = 3200$, shows a constant amplitude of entropy wave downstream of the shock. It is also observed that amplitude of entropy perturbation is actually reduced after interacting with shock. The coarser grid solutions corresponding to $N = 800$, $N = 400$ and $N = 200$ show increasingly dissipative characteristics. The amplitude of refracted entropy wave is reduced continuously as distance from main shock increase. However, it is important to note that near the fitted shock, results are very good and almost similar for all the grid resolutions used.

All in all, the problem of one dimensional interaction of shock and density disturbance solved by high-order shock fitting algorithm matches well to the results available in the literature.

Moreover, the results were found to be remarkably good near the main shock even for very coarse grid. This is in contrast to shock capturing schemes which suffer most dissipation around strong discontinuity.

6 TWO-DIMENSIONAL SHOCK AND TURBULENCE INTERACTION PROBLEM

In the literature, results are available for small two-dimensional vorticity and entropy disturbances interacting with a shock which we have used for assessing utility of our shock-fitting algorithm for shock-turbulence interactions. Mahesh [17] carried out linear interaction analysis for two-dimensional problem of a normal Mach 1.5 shock interacting with weak plane vorticity-entropy waves traveling at varying angles of incidence. For this problem, the domain is assumed to contain an ideal gas with specific heat ratio 1.4. Fluctuations are superposed over steady Mach 1.5 normal shock solutions (obtained from the Rankine-Hugoniot relations) for the gas. In a shock capturing setting, disturbances propagate downstream from the inflow boundary and interact with the normal shock as shown Fig. 11(a). The interactions of normal shock and disturbances cause time-periodic shock distortions and disturbance amplifications.

A typical study with shock-capturing requires solving for flow upstream as well as downstream of the shock. However, our conventional shock-fitting algorithm can find effect of given upstream disturbances on downstream flow without solving for flow coming into the shock. Hence, we solve only for the flow which has passed through shock as was actually done by Mahesh for linear analysis. The computational domain used for this study is shown in Fig 11 (b). To use conventional moving-grid shock-fitting algorithm, a stationary Mach 1.5 shock wave is perturbed at $t = 0.0$ by a small amplitude disturbance field of the incident plane wave that makes angle ψ_1 with the X- axis. The incident field has the following form:

$$\begin{aligned} u' &= U_1 A_v \sin\psi_1 \cos(k_x x + k_y y - U_1 k_x t) \\ v' &= -U_1 A_v \cos\psi_1 \cos(k_x x + k_y y - U_1 k_x t) \\ \rho' &= \rho_1 A_v \cos\psi_1 \cos(k_x x + k_y y - U_1 k_x t) \\ p' &= 0.0 \end{aligned} \tag{29}$$

where variables U and ρ denote the mean velocity and density respectively and The variables u', v', p' and ρ' represent fluctuations in velocities, pressure and density respectively. Subscripts 1 and 2 denote the upstream and downstream steady states. For the computations presented here, $k_y = k\sin\psi_1 = 1$ and $k_x = k\cos\psi_1$ is used. Length of domain in y direction, $L_y = 2\pi$ ensures that each x location the flow is periodic over the computation domain in Y direction. The variables used here were non-dimensionalized by appropriate combinations of reference length L^*_0, reference speed of sound c^*_0 and reference density ρ^*_0. Here c^*_0 and ρ^*_0 correspond to the unperturbed free-stream values. For the present study we used $A_v = A_e = 0.025$, i.e. vorticity and entropy waves in same phase were considered.

The problem was computed by solving Euler equations with our conventional moving-grid two-dimensional shock-fitting algorithm. Periodic boundary conditions were used in Y-irection. In streamwise direction (X), the shock forms the inflow boundary which is solved by the shock-fitting algorithm. As computations are started, large oscillations in flow properties are observed downstream of the shock along all values of Y coordinates. These disturbances propagate downstream followed by an oscillating field. Figure 12 shows transients in vorticity profiles moving downstream of the flow. The exit boundary presents a problem for computation since flow is subsonic at the exit. Boundary conditions at the exit need to be chosen such that vorticity, acoustic and entropy perturbation in the domain are allowed to propagate properly otherwise such disturbances might reflect and contaminate the solution. We use approximately non-reflecting boundary conditions of Poinsot and Lele [48] at the outflow boundary and found that vorticity waves leave the domain and we obtain time periodic vorticity downstream of the shock. Figure 13 shows vorticity profile after the transients leave the domain. It can be seen that a sinusoidal vorticity profile is obtained along X direction at all locations.

Validation of the results obtained for the problem considered can be done against the theoretical and numerical studies performed by Mahesh [17]. Mahesh considered linearized Euler equations (linearized about the uniform flow) behind the shock and solved a boundary-value problem for the shock displacement and the flow behind the shock wave. It was found that the solution behind the shock wave has two different regimes that differ in nature of the pressure field. For a given Mach number, the two regimes are demarcated by a critical angle of incidence denoted by ψ_c. If angle of incidence is less than critical angle of incidence, the pressure field is a plane wave. However, if $\psi_c < \psi_1 < \pi/2$ the pressure field behind the shock wave decays exponentially. Linear analysis of Mahesh predicts a value of 61.36° for critical incidence angle for Mach 1.5 flow. Linear theory also predicts that velocity and entropy fields behind the shock waves should be plane waves over both the regimes. This information from linear theory was used to qualitatively validate our results. Figure 14 shows pressure in X direction along the mid-plane of the domain for various angles of incidence. It can be seen that pressure profile is sinusoidal for $\psi_1 = 15°$ and $\psi_1 = 45°$. Also, the wavelength for oscillation in X direction is significantly larger for the case of $\psi_1 = 45°$ as compared to solutions corresponding to $\psi_1 = 15°$. This is also confirmed by the linear theory results of Mahesh as wavenumber in X direction is proportional to $\cos\psi_1$ for a fixed Mach number of the incoming flow. It is also observed by our studies (Figs. 14(c) and 10(d)) that pressure goes towards an asymptotic value (which is the mean downstream value) and thus perturbation decreases exponentially. Figure 15 shows variation of vorticity in X-direction along midplane of domain, $Y = \pi$. It can be seen that all the profiles show sinusoidal variations. Similar to the pressure waves, for the cases of less than critical incident angle the wavelength of X direction oscillations should increase with increase in incidence angle which is indeed the case here. Apart from vorticity disturbances, entropy disturbances also interact with the shock in present case. Linear study predicts a plane wave structure for disturbance waves. Figure 16 presents variation of entropy as defined in Eq. (28) along streamwise direction at mid-plane of the domain. It is clearly seen that entropy perturbation downstream of the shock is a plane wave for all incident angles. Thus, while the pressure perturbations show different behaviors in the two regimes, vorticity and entropy perturbations remain sinusoidal. This behavior is predicted by the linear theory as well and thus qualitatively confirms the validity of the results obtained from shock-fitting computations.

Linear theory by Mahesh [17] provides the amplification factors for perturbation in vorticities, $\overline{\omega'^2_2}/\overline{\omega'^2_1}$. As shown in Fig. 16, vorticity perturbations downstream of the flow are plane waves for all angles of incidence. After the initial transient left the domain, statistics gathered over a period of inflow disturbance $2\pi/U_1 k_x$ were analyzed for amplification of disturbance in vorticity. Table 1 compares the amplification factors, $\overline{\omega'^2_2}/\overline{\omega'^2_1}$ obtained from our shock-fitting solution to the numerical and theoretical solution given by Mahesh.

Table 1: Comparison of amplifications in vorticity fluctuations $\overline{\omega'^2_2}/\overline{\omega'^2_1}$ as obtained from different methods.

Angle	Shock Fitting	Mahesh (Computational)	Linear Theory
0˚	3.47	3.43	3.45
15˚	4.06	4.05	4.07
45˚	5.27	5.22	5.26
61.36˚	8.1	6.89	8.5
75˚	4.52	4.6	4.53
85˚	3.85	-	3.8

The tabulated results are also plotted against the linear theory results provided by Mahesh in Fig. 17. It is observed that for most of the cases, our results show great agreement with the linear theory solutions.

Thus we see that for two-dimensional calculations our results from conventional shock-fitting are in qualitative and quantitative agreement with linear theory results. Moreover, the shock-fitting results behind the shock for all the incidence angles of disturbances are free from any spurious numerical oscillations. This is significant considering that shock capturing schemes may incur such oscillations in presence of shock as shown by Lee and Zhong [3].

7 CONVERGENCE OF THE 5TH ORDER SHOCK-FITTING METHOD

The focus of this study is on the high-order shock-fitting methodology for disturbance interactions with shock. In literature, generally design accuracy for the method is shown only with the simple and smooth problems. There are very few studies which consider convergence properties of schemes with non-linear discontinuities like shocks. Casper and Carpenter [43, 49] considered shock-disturbance interaction problems with shock capturing schemes and found only first order convergence in the smooth post-shock flow even with high order schemes. In general, shock-capturing methods suffer from reduction in accuracy in post-shock flow-fields. Hence, it is important to ensure that design accuracy is indeed achieved with high-order shock-fitting method for shock-disturbance interaction problems. Shu-Osher problem of section 5 is not a very good problem for convergence study as disturbance traveling towards shock creates a sudden jump in density at initial moment and small shocklets and expansion waves are formed behind the shock.

Suresh [50] used a variation of shock-fitting method (by adding grids instead of moving the grid) to show 3rd order accuracy of a shock-disturbance problem. This problem is a modified form of Shu-Osher problem and has smooth profile behind the main shock. We also consider the same problem with our shock-fitting schemes that use 5th order upwind method in interior with 4th order at the shock-boundary. Problem is one dimensional interaction of shock with a density disturbance which is defined as follows:

At $t = 0$ for $x < 0.4$ we have

$$\begin{aligned} \rho &= (\gamma+1)M^2 \Big/ \left[(\gamma-1)M^2+2\right] \\ u &= 2\gamma^{1/2}\left(M^2-1\right)\Big/\left[(\gamma+1)M\right] \\ p &= 1+2\gamma\left(M^2-1\right)\Big/(\gamma+1) \end{aligned} \tag{30}$$

while for $x > 0.4$, we have

$$\begin{aligned} \rho &= 1.0+\varepsilon\sin^4(2.5\pi x) \\ u &= 0.0 \\ p &= 1.0 \end{aligned} \tag{31}.$$

Here we use a strong shock with M=3 , γ=1.4, ε=0.2 . ρ, γ, u, M and p represent density, ratio of specific heats for the gas, velocity, Mach number and pressure respectively. This problem is a modified form of more popular Shu-Osher problem and has been chosen since post shock flow for this problem have continuity in density as well as its first, second and third derivatives in space, thus making post-shock solution much smoother. The unsteady problem is computed till $t = 0.32$ so that shocklets are not formed behind the main shock. Thus the problem is expected to show true order of convergence for the shock-fitting method. To carry out the convergence analysis, we compute the unsteady problem for a number of grid-sets. Error from Richardson extrapolate is considered for finding the approximate order of convergence. Thus error for a grid spacing of $\Delta x/2$ for a variable u is defined as,

$$e_{\Delta x/2} = \frac{1}{2^n-1}\left|u_{\Delta x/2}-u_{\Delta x}\right|, \tag{32}$$

where $u_{\Delta x/2}$ and $u_{\Delta x}$ are solution for variable u from grids of spacings of Δx and $\Delta x/2$ respectively and n is expected order of accuracy (n = 5 in our case). The error values are obtained for different sets of grids and the approximate order of accuracy, n, is then defined as:

$$n = \log\left(\frac{e_{\Delta x}}{e_{\Delta x/2}}\right)\Big/\log(2) \tag{33}.$$

7.1 Convergence analysis for new front-tracking based fixed grid shock-fitting method

For the conventional shock-fitting, it is advisable to solve the above problem in the reference frame where shock movements are nominal since large movements in the grid would affect the accuracy. However, when applying fixed grid shock fitting method described in section 4, we do not have such restriction. Hence the problem is solved in the reference frame

described by Eq. (30) and (31) i.e. a Mach 3 shock moves in still fluid with density disturbances. This method uses 5th order upwind finite difference scheme in interior with 4th order one-sided difference scheme around the shock. No additional dissipation is applied except that already present in original 5th order upwind scheme as given in (21). RK-1 time integration is used with small enough time-step so that temporal errors do not affect the overall accuracy significantly. We use our two-dimensional fixed grid shock-fitting code based on front tracking algorithm to solve this problem for 4 sets of grids:

$$\begin{aligned}
&\text{Grid-set 1: Spacing, } dx_1 = 5\times10^{-3} \quad \text{(No of grids, N=400)}\\
&\text{Grid-set 2: Spacing, } dx_2 = 2.5\times10^{-3} \quad \text{(No of grids, N=800)}\\
&\text{Grid-set 3: Spacing, } dx_3 = 1.25\times10^{-3} \quad \text{(No of grids, N=1600)}\\
&\text{Grid-set 4: Spacing, } dx_4 = 6.25\times10^{-4} \quad \text{(No of grids, N=3200)}
\end{aligned} \tag{34}$$

Fig. 18 shows density profile at final time for three sets of grids (grid-set 2 to 4). In full view (Fig. 18(a)) the solutions look barely different from each other. However, as we zoom in on the solution we see small differences in the solutions (see Fig. 18(b) and 18(c)). It can be noticed that as we refine the grid, the solutions are obviously converging. Moreover, it can be also deduced from Fig. 18(b) and 18(c) that convergence rate is definitely better than 1st order. To investigate convergence, we find the error values from Richardson extrapolate as defined by Eq. (32) for different grid spacings. Spatial variations of point-wise errors obtained this way for grid-spacings dx_3 and dx_4 are compared in Fig. 19 for density as well as velocity values. It can be observed that errors for finer grid are significantly less. Since log of error values on base 2 is plotted, one can deduce the local order of convergence, as defined in (33) , by taking difference between the two profiles in Fig. 19. It can be seen that both velocity and density results show is mostly 5th order rate of convergence at all spatial points. To quantify the global error, we take 2-norm of local error values as defined by (32) and find the approximate error of convergence from Eq. (33) for different sets of grids. These values are tabulated in table 2.

Table 2: Order of convergence using fixed grid shock-fitting for problem defined by (30)*and* (31)

	Error I: e_{dx_2}	Error II: e_{dx_3}	Error III: e_{dx_4}	Order from I and II	Order from II and III
Density	3.48E-05	1.73E-06	9.16E-08	4.34	4.24
Velocity	5.55E-07	1.81E-08	5.77E-10	4.94	4.97
Pressure	4.29E-06	1.43E-07	4.68E-09	4.91	4.93
Shock-location	2.81E-08	7.48E-10	4.48E-11	5.23	4.07

From Table 2 it is observed that the method shows a convergence rate between 4th and 5th order. This is expected from our method which uses 5th order upwind scheme in the interior with 4th order one-sided difference around the shock. Moreover, the shock-fitting solution does not incur spurious oscillations around the shock. This provides ample evidence of the advantages of using shock-fitting method for the problems where simple shock geometries are involved.

7.2 Convergence properties using conventional moving- grid shock-fitting

When shock-fitted grids are used for computations to solve the problem given by Eqs. (30) and (31), we solve the problem in the reference frame of steady shock moving with shock velocity, $M\gamma^{1/2}$. The shock now forms boundary of the computational domain at $x = 2$ while conditions given by Eq. (31) are imposed as space and time depended freestream disturbances given by:

$$\begin{aligned} \rho_\infty &= 1.0 + \varepsilon \sin^4 \left\{ 2.5\pi \left(x + M\gamma^{1/2} t \right) \right\} \\ u_\infty &= -M\gamma^{1/2} \\ p_\infty &= 1.0 \end{aligned} \tag{35}$$

It is important to observe that by using freestream disturbances given by Eq.(35), we are able to solve the same problem in mean-shock-reference frame as we solved with fixed grid front-tracking method in section 7.1. We solve this problem using conventional shock-fitting method till time, $t = 0.32$. With shock fitting we use 5th order upwind finite difference scheme in the interior while using one sided 4th order scheme at the boundary. There is no artificial dissipation use apart from the one inherent in the upwind scheme. An RK-2 method is used for time integration. Time step is taken very small so that there is no significant temporal error effects on accuracy of the problem. The results are presented in Fig. 20 for density variation using three sets of grids. It can be observed that results are fairly indistinguishable from each other in full view. As we zoom in on the different portions of the density profiles, it is observed that results are converging with grid refinement (20(b) and 20(c)).

Table 3: Order of convergence using shock-fitted moving grid method for problem defined by (35)

	Error I: e_{dx_2}	Error II: e_{dx_3}	Order from I and II
Density	2.53E-05	8.77E-07	4.85
Velocity	1.48E-06	4.87E-08	4.92
Pressure	1.14E-05	3.74E-07	4.93
Shock-location	3.15E-08	7.84E-10	5.33

As explained before, we take difference between results while successively refining the grids and find error values as defined by (32) for flow variables to assess convergence of the method. Such point-wise errors for density and velocity values are plotted as spatial variation in Fig. 21 for grid spacings $dx_2=2.5\times10^{-3}$ and $dx_3=1.25\times10^{-3}$. Similar to Fig. 19, we plot log of error values on base 2. Hence, one can obtain local order at any point by just taking difference between the two curves corresponding to different grid spacings. It is observed that error values are definitely much smaller for the finer grid and local order is around 5 for most of the points. Global accuracy is obtained by taking 2-norm of these local errors for different grid-sets and finding convergence rates as defined in Eq.(33). These values are tabulated in Table 3.

It is observed from Table 3 that design accuracy (5^{th} order) is indeed achieved using the conventional moving-grid shock-fitting method. Comparing with same values from Table 2, we see that error values for both the methods is approximately of the same order, although conventional shock-fitting method shows slightly better results. The error values presented here are significantly smaller than those obtained from shock-capturing schemes presented by Suresh [50]. For example table 3 of Ref [50], shows an error of around 10^{-5} (according to definition given by (32))in velocity values for 5^{th} order shock-capturing scheme with grid spacing of $dx_3=1.25\times10^{-3}$ while corresponding errors from shock-fitting results (table 2 and table 3) are around 10^{-8}. Thus significantly better results are obtained as compared to shock-capturing schemes for this canonical problem.

Thus, our shock-fitting method shows high-order accuracy with conventional moving grids as well as new fixed-grid setting. Such result is very important considering the fact that the problem is actually strongly non-linear with a Mach-3 shock and shock capturing schemes suffer from reduction in accuracy for such problems as shown above. Thus shock-fitting methodology offers a high-order alternative for the cases where it can be applied. It is especially encouraging to obtain high-order accuracy from the shock-fitting in the fixed grid setting since it allows shock to move through the underlying grid; making it applicable to a lot of problems that are not suitable for conventional moving-grid shock-fitting method.

8 SUMMARY AND FUTURE WORK

From the results in the current study, we observe that results produced from our high-order shock fitting algorithm agrees well with those available in literature for simple cases of shock and disturbance interactions. For the Shu-Osher problem, very accurate results are obtained near the main shock even for a coarse grid which in contrast to dissipative solutions obtained from shock capturing for similar grids. For 2-D interactions of shock and vorticity-entropy wave, results from shock-fitting algorithm agree well with the predictions of linear interaction analysis.

We have also shown the feasibility of using fixed grid algorithms with the shock-fitting algorithm. Moreover, 5^{th}-order convergence of conventional as well as front-tracking based fixed-grid shock-fitting methods has also been established. This confirms a major advantage of using shock-fitting method over shock capturing methods to obtain high order accuracy as desired in numerical simulations of shock-turbulence interactions.

In future, we will further develop our fixed grid shock-fitting method to make it more robust and efficient. We intend to extend this shock-fitting method to include new immersed interface algorithm of Zhong [1, 2]. At shocks, this immersed interface algorithm requires jumps only in values of flow variables and their derivatives while giving arbitrarily high-order accuracy. Thus, compared to other Cartesian grid methods, this method is more suitable for high-order computations of physical problems. Such high-order implementation, if successful, will be very helpful in solving other multi-phase problems as well.

9 ACKNOWLEDGEMENTS

This research is supported by DOE Office of Science as part of a SciDAC (Scientific Discovery through Advanced Computing) project with "Science Application" in Turbulence. The authors would like to thank Prof. S. K. Lele and Prof. P. Moin of the Stanford University; Drs. A. Cook, W. Cabot, B. Sjögreen of the Lawrence Livermore National Laboratory and Dr. H. C. Yee of the NASA Ames Research Center for their valuable suggestions during the course of this work.

REFERENCES

1. Zhong, X., *A new high-order immersed interface method for multi-phase flow.* AIAA paper 2006-1294, 2006.
2. Zhong, X., *A new high-order immersed interface method for solving elliptic equations with imbedded interface of discontinuity.* Journal of Computational Physics, 2007. **In Press.**(Corrected proof available online 30 January 2007).
3. Lee, T.K., and Zhong, X., *Spurious numerical oscillations in simulation of supersonic flows using shock-capturing schemes.* AIAA Journal, 1999. **37**(3): p. 313-319.
4. Kovasznay, L.S.G., *Turbulence in supersonic flow.* Journal of the Aeronautical Sciences, 1953. **20**(10): p. 657-682.
5. Chu, B.T., and Kovasznay, L. S. G., *Nonlinear interactions in a viscous heat-conducting compressible gas.* Journal of Fluid Mechanics, 1958. **3**: p. 494-514.
6. Ribner, H.S., *Convection of a pattern of vorticity through a shock wave.* NACA TN-2864 (Also as NACA Report 1164 1953), 1953.
7. Ribner, H.S., *Shock-turbulence interaction and the generation of noise.* NACA TN-3255 (Also as NACA Report 1233), 1954.
8. Ribner, H.S., *Acoustic energy flux from shock-turbulence interaction.* Journal of Fluid Mechanics, 1969. **35**: p. 299-310.
9. Moore, F.K., *Unsteady oblique interaction of a shock wave with a plane disturbances.* NACA TN-2879 (Also as NACA Rep. 1165), 1953.
10. Kerrebrock, J.L., *The interaction of flow discontinuities with small disturbances in a compressible fluid*, in *Mechanical Engineering*. 1956, California Institute of Technology: Pasadena, CA.
11. McKenzie, J.F., and Westphal, K. O., *Interaction of linear waves with oblique shock waves.* Physics of Fluids, 1968. **11**: p. 2350-2362.
12. Goldstein, M.E., *Turbulence generated by the interaction of entropy fluctuations with non-uniform mean flows.* Journal of Fluid Mechanics, 1979. **93**: p. 209-224.

13. Lee, L., Moin, P., and Lele, S. K., *Interaction of isotropic turbulence with a shock wave.* Report TF-52. Dept. Mech. Eng., Stanford Univ., CA, 1992.
14. Lee, L., Lele, S. K., and Moin, P., *Direct numerical simulation of isotropic turbulence interacting with a weak shock wave.* Journal of Fluid Mechanics, 1993. **251**: p. 533-562.
15. Lee, L., Lele, S. K., and Moin, P., *Interaction of isotropic turbulence with a strong shock wave.* AIAA Paper 94-0311, 1994.
16. Mahesh, K.A., Lee, L., Lele, S. K., and Moin, P., *The interaction of an isotropic field of acoustic waves with a shock wave.* Journal of Fluid Mechanics, 1995. **300**: p. 383-407.
17. Mahesh, K.A., Moin, P., and Lele, S. K., *The interaction of a shock wave with a turbulent shear flow.* Report TF-69, Thermosciences Division, Mechanical Engineering Department, Stanford University, 1996.
18. Mahesh, K.A., Lele, S. K., and Moin, P., *The influence of entropy fluctuations on the interaction of turbulence with a shock wave.* Journal of Fluid Mechanics, 1997. **334**: p. 353-379.
19. Fabre, D., Jacquin, L., Garnier, E., and Sagaut, P. . *Linear interaction analysis: The effect of a shock wave on a homogeneous perturbation field and on an entropy spot*. in *High Speed Compressible Flows, Euromech 403*. 1999. Poitiers.
20. Fabre, D., Jacquin, L., and Sesterhenn, J., *Linear interaction of a cylindrical entropy spot with a shock.* Journal of Physics of Fluids A, 2001. **13**(8): p. 2403-2422.
21. Pao, S.P., and Salas, M. D., *A numerical study of two-dimensional shock vortex interaction.* AIAA Paper 81-1205, 1981.
22. Zang, T.A., Hussaini, M. Y., and Bushnell, D. M. , *Numerical Computations of Turbulence Amplification in Shock-Wave Interactions.* AIAA Journal, 1984. **22**(1): p. 13-21.
23. Hussaini, M.Y., Kopriva, D., Salas, M. D., and Zang, T. A., *Spectral methods for the Euler equations. II - Chebyshev methods and shock fitting.* AIAA Journal, 1987. **23**: p. 234-240.
24. Meadows, K.R., Kumar, A., and Hussaini, M. Y., *Computational Study on the Interaction between a vortex and a shock Wave.* AIAA Journal, 1991. **29**(2): p. 174-179.
25. Meadows, K.R., and Casper, J., *Computing unsteady shock waves for aeroacoustic applications.* AIAA Paper 1993-4329, 1993.
26. Grasso, F., and Pirozzoli, S. , *Shock-wave-vortex interactions: shock and vortex deformations, and sound production.* Theoretical and Computational Fluid Dynamics, 1993. **13**(6): p. 421-456.
27. Andreopoulos, Y., Agui, J. H., and Briassulis, G., *Shock wave-turbulence interactions.* Annual Review of Fluid Mechanics 2000. **32**: p. 309-345.
28. Hannappel, R., and Friedrich, R., *Direct numerical simulation of a Mach 2 shock interacting with isotropic turbulence.* Applied Scientific Research, 1995. **54**: p. 205-221.
29. Jamme, S., Cazalbou, J. B., Torres, F., and Chassaing, P., *Direct numerical simulation of the interaction between a shock wave and various types of isotropic turbulence.* Flow, Turbulence and Combustion, 2202. **68**: p. 227-268.
30. Adams, N.A., and Shariff, K., *A high-resolution hybrid compact-ENO scheme for shock turbulence interaction problems.* Journal of Computational Physics, 1996. **127**(27): p. 57-.
31. Adams, N.A., and Shariff, K., *Direct numerical simulation of turbulent compression corner flow.* Theoretical and Computational Fluid Dynamics, 1998. **12**: p. 109-129.

32. Pirozzoli, S., *Conservative hybrid compact-WENO schemes for shock-turbulence interaction.* Journal of Computational Physics, 2002. **178**(1): p. 81-117.
33. Ducros, F., Ferrand, V., Nicoud, F.,Weber, C., Darracq, D., Gacherieu C., and Poinsot, T., *Large eddy simulation of the shock/turbulence interaction.* Journal of Computational Physics, 1999. **152**: p. 517-549.
34. Yee, H.C., Sandham, N .D., and Djomehri, M. J. , *Low dissipative high-order shock capturing methods using characteristic based filters.* Journal of Computational Physics, 1999. **150**: p. 199-238.
35. Sjogreen, B., and Yee, H. C., *Multiresolution wavelet based adaptive numerical dissipation control for high order methods.* Journal of Scientific Computing, 2004. **20**(2): p. 211-215.
36. Cook, A.W., *Comparison of modern methods for shock hydrodynamics.* LLNL report no. UCRL-PROC-212901, 2005.
37. Cook, A.W., Cabot, W. H., Welcone, M. L., Williams, P. L., Miller, B. J., de Supinski B. R., and Yates, R. K., *Tera-scalable algorithms for variable-density elliptic hydrodynamics with spectral accuracy.* LLNL report no. UCRL-CONF-211384, 2005, 2005.
38. Ma, Y., and Zhong, X., *Receptivity of a Supersonic Boundary Layer over a Flat Plate. Part 3: Effects of Different Types of Free-Stream Disturbances.* Journal of Fluid Mechanics, 2005. **532**: p. 63-109.
39. Ma, Y., and Zhong, X., *Receptivity of a Supersonic Boundary Layer over a Flat Plate. Part 1: Wave Structures and Interactions.* Journal of Fluid Mechanics, 2003. **488**: p. 31-78.
40. Ma, Y., and Zhong, X., *Receptivity of a Supersonic Boundary Layer over a Flat plate. Part 2: Receptivity to Freestream Sound.* Journal of Fluid Mechanics, 2003. **488**: p. 79-121.
41. Wang, X., and Zhong, X., *Numerical Simulation and Experiment Comparison of Leading-Edge Receptivity of A Mach 5.92 Boundary Layer*, in *44th AIAA Aerospace Sciences Meeting and Exhibit*. 2006, AIAA paper 2006-1107.
42. Sesterhenn, J., *Direct numerical simulation of the interaction of isotropic turbulence with a shock wave using shock-fitting.* Comptes rendus. Mecanique [1631-0721], 2005. **333**(1): p. 87-93.
43. Carpenter, M.H., and Casper, J. H., *Accuracy of shock capturing in two spatial dimensions.* AIAA Journal, 1999. **37**(9): p. 1072-1079.
44. Unverdi, S.A., and Tryggvason, G. , *A front-tracking method for viscous, incompressible, multi-fluid flows.* Journal of Computational Physics, 1992. **100**(1): p. 25-37.
45. Zhong, X., *High-order finite-difference schemes for numerical simulation of hypersonic boundary-layer transition.* Journal of Computational Physics, 1998. **144**: p. 662-709.
46. Shu, C.W., and Osher, S., *Efficient implementation of essentially nonoscillatory shock-capturing schemes,II.* Journal of Computational Physics, 1989. **83**(1): p. 32-78.
47. Visbal, M.R., and Gaitonde, D. V., *Shock capturing using compact-differencing-based methods* AIAA-2005-1265, 2005.
48. Poinsot, T.J., and Lele, S. K., *Boundary conditions for direct simulations of compressible viscous flow.* Journal of Computational Physics, 1992. **101**(1): p. 104-129.
49. Casper, J., and Carpenter, M. H.,, *Computational Considerations for the Simulation of Shock-Induced Sound.* . SIAM Journal of Scientific Computing, 1998. **19**(3): p. 813-828.

50. Suresh, A., *Interaction of a shock with a density disturbance via shock fitting* Journal of Computational Physics, 2005. **206**: p. 6-15.

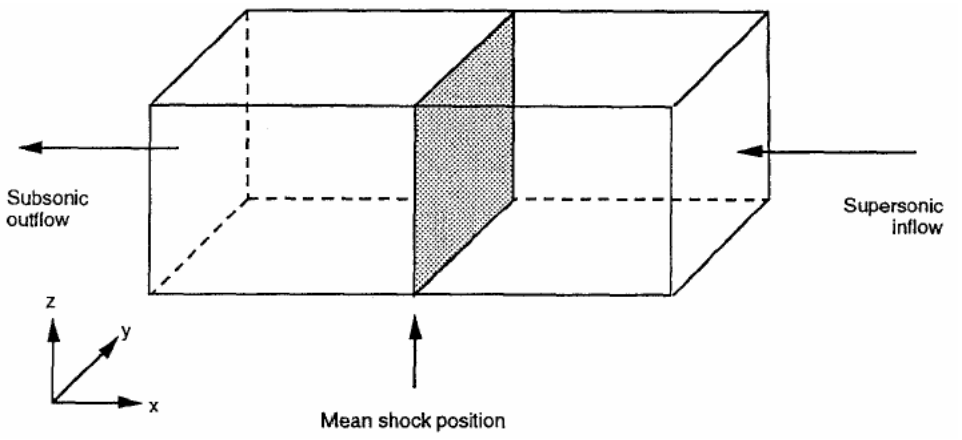

Fig. 1: A Schematic of typical setting of shock and disturbance/ turbulence interaction

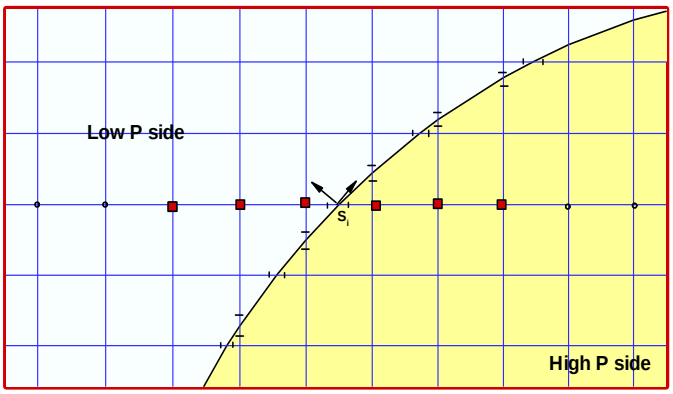

Fig. 2: Irregular points for 5th order fixed grid shock-fitting based on front tracking.

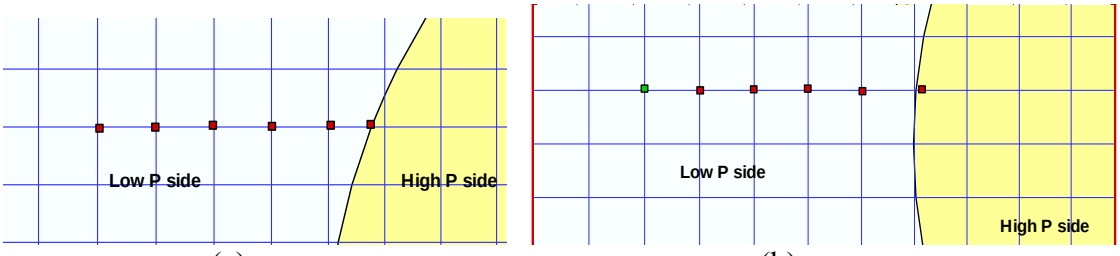

(a) (b)

Fig.3: (a) Non-uniform stencil used for one-sided difference scheme. (b) Derivatives are not computed at the point closest to interface and an extra point (green) is included in the stencil for one-sided difference.

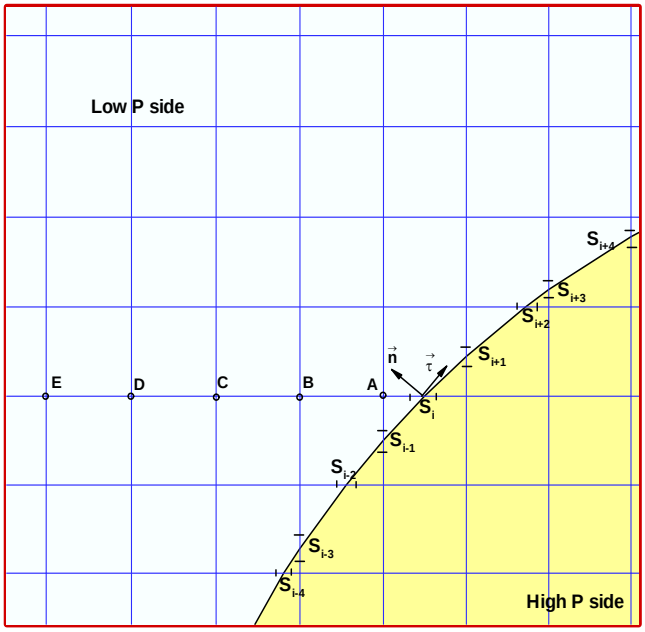

Fig. 4. Schematic for arrangement of Marker Points and stencil for one-sided differentiation for the fixed-grid-shock-fitting methodology.

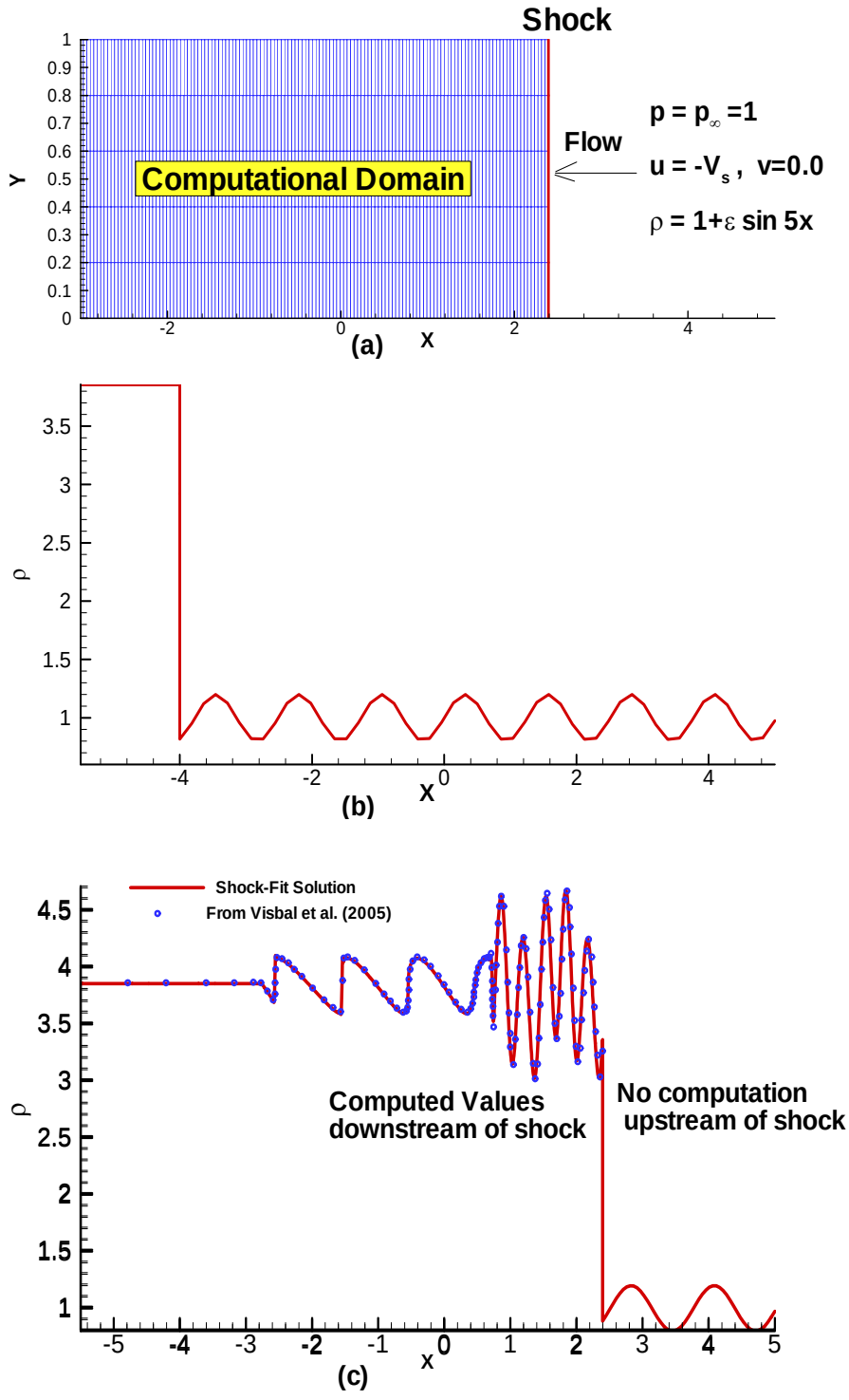

Fig. 5: For computation of Shu-Osher Problem using conventional shock-fitting (a) 2D computational domain (b) Initial density profile (c) Density profile at t=1.8 (solid line) compared with shock-capturing solution (dots).

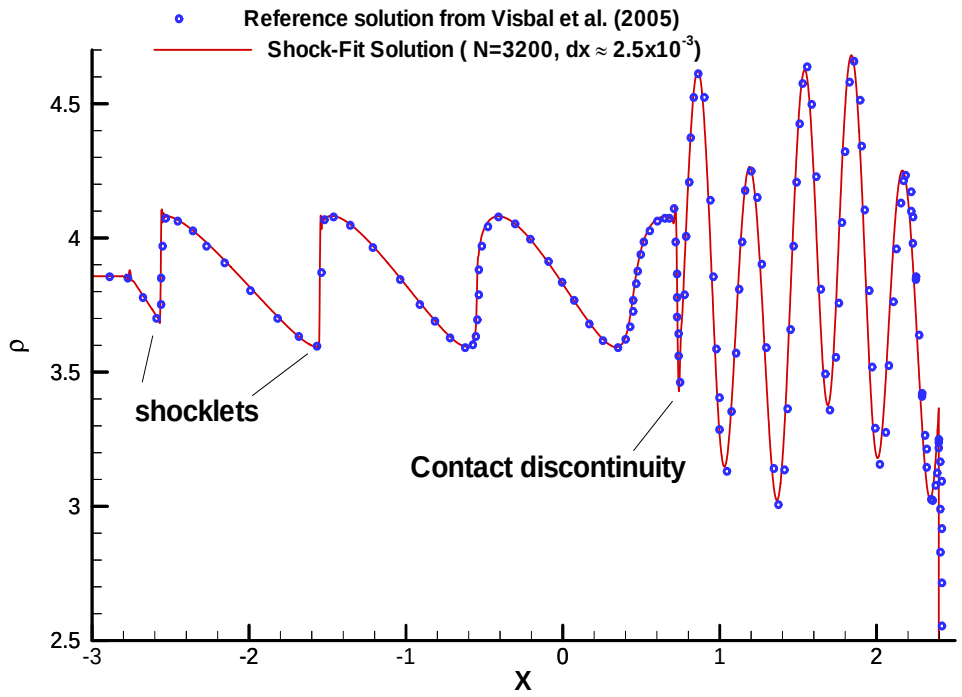

Fig. 6: A zoomed view of comparison of shock-fitted density profile (solid) at t = 1.8 against the fine-grid solution (dots) of Visbal et al.(2005).

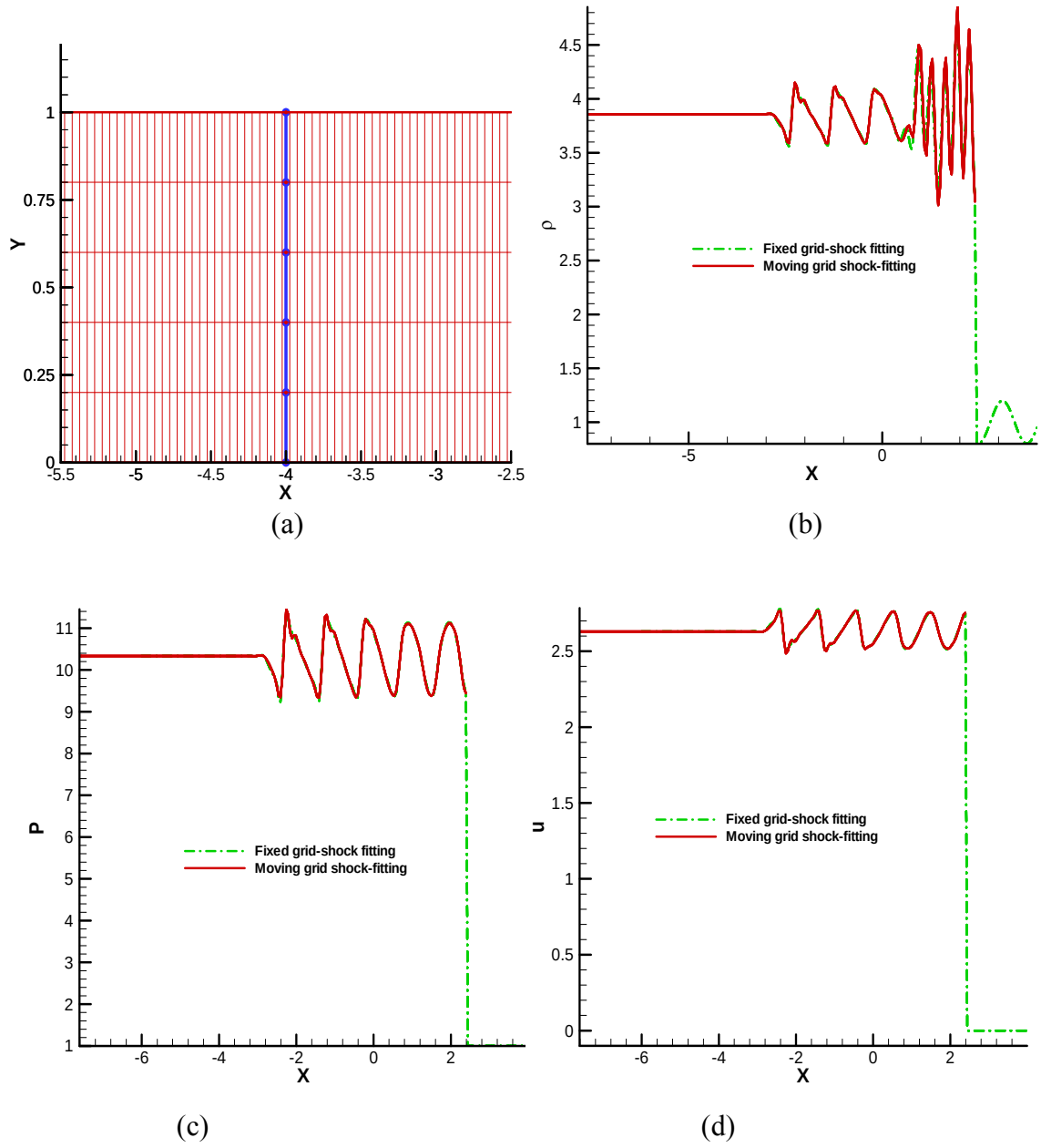

Fig. 7: (a) A zoomed view of marker points (blue) and grids (red) at initial time step for computation of shu-osher problem with fixed grid shock-fitting method. Comparison of solutions obtained for front-tracking based fixed-grid shock-fitting and conventional moving-grid shock-fitting for (b) Density (c) Pressure and (d) velocity.

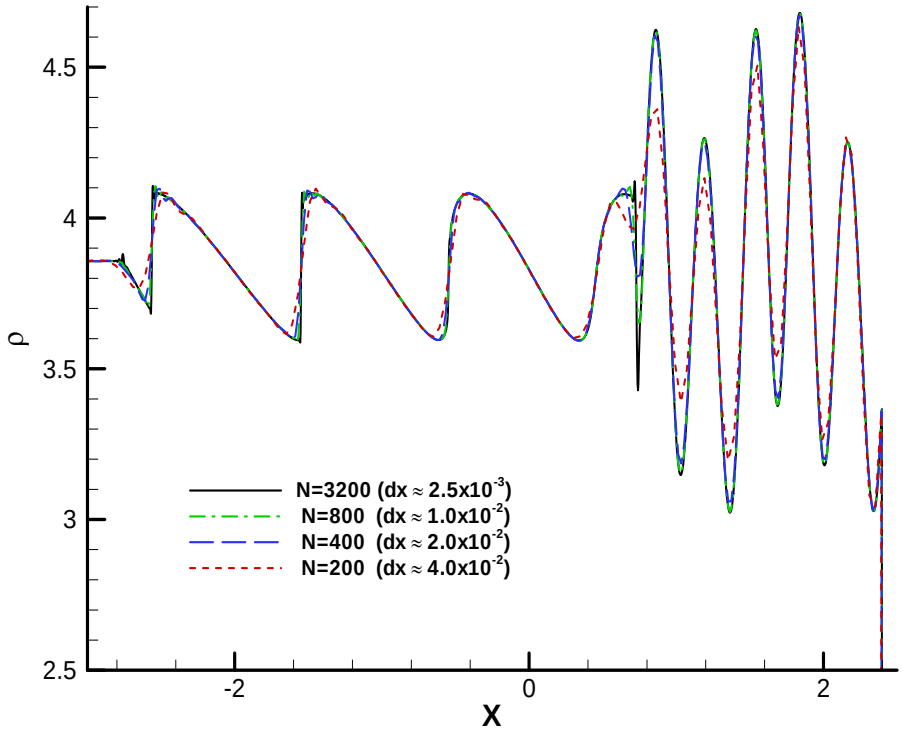

Fig. 8: Effect of grid refinement on density profile at t = 1.8 using conventional shock-fitting

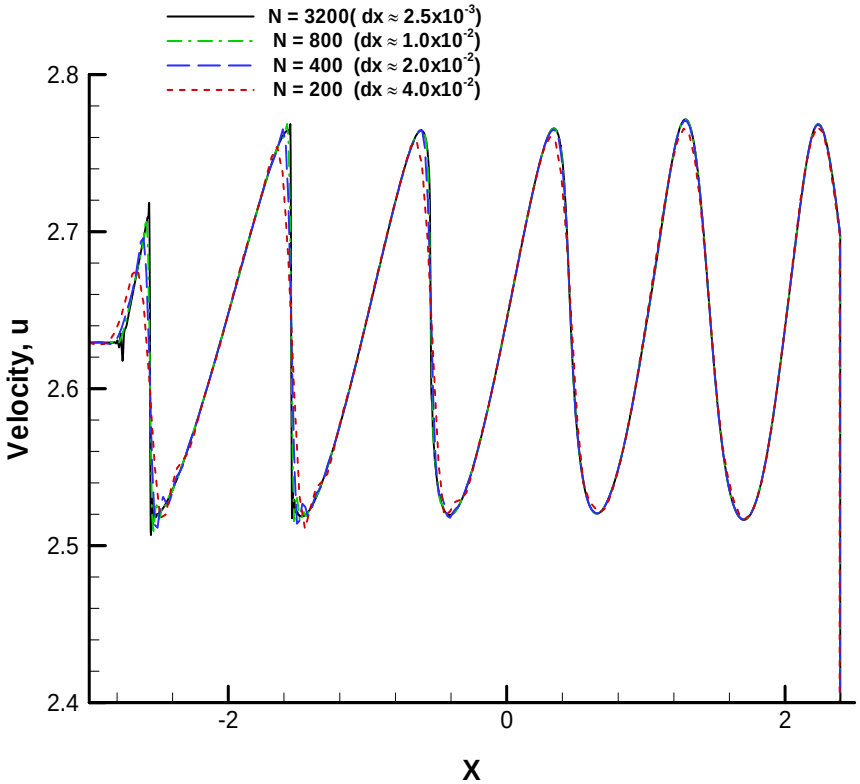

Fig. 9: Effect of grid refinement on velocity profile at t = 1.8 (using conventional shock-fitting).

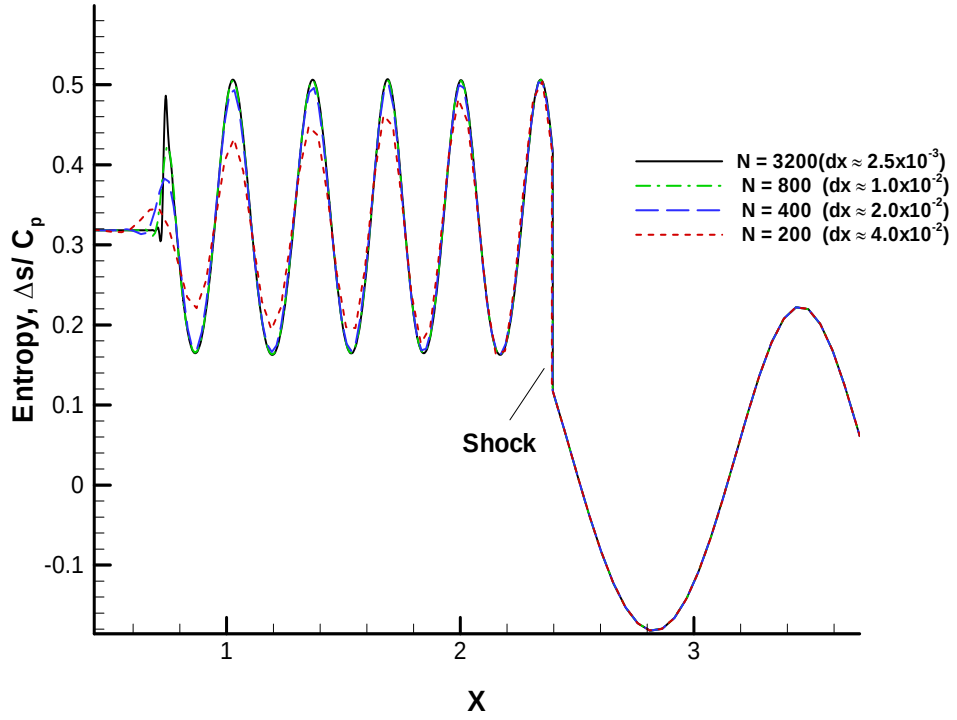

Fig. 10: Effect of grid refinement on entropy profile at t = 1.8 (using conventional shock-fitting).

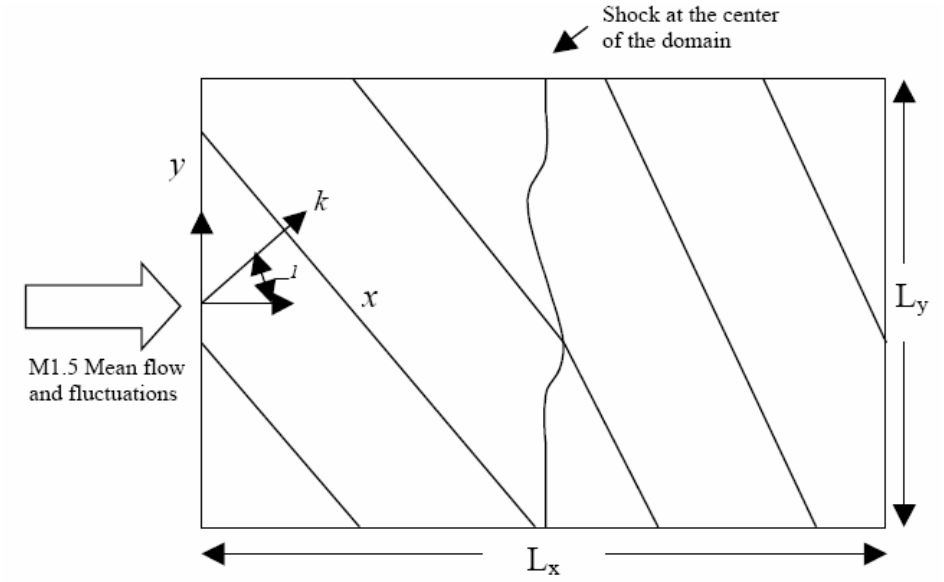

(a)

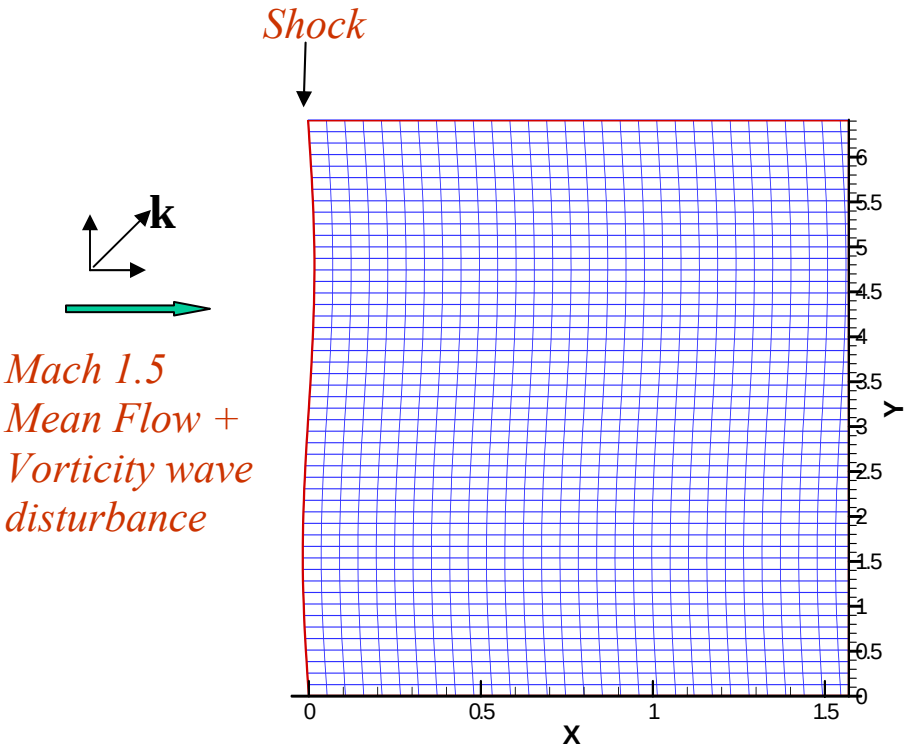

(b)

Fig. 11: For the shock and vorticity-entropy wave interaction (a) Schematic of the problem and (b) Computational domain used for conventional shock-fitting algorithm. Shock forms the left boundary in (b) where oscillations in shock can be noticed.

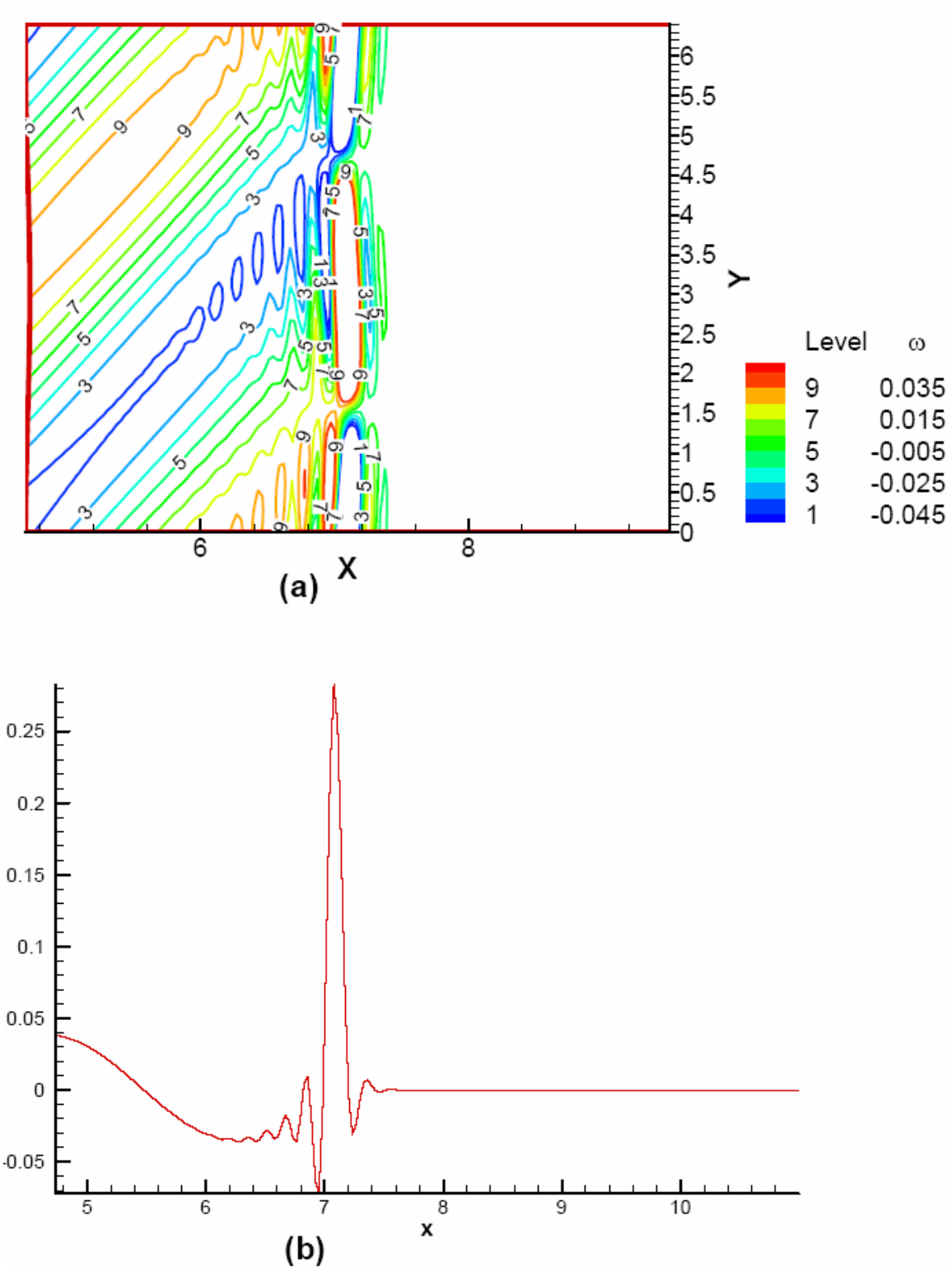

Fig. 12: Interaction of a vorticity-entropy wave at t = 5.0 after start (a) Contours of vorticity (b) Variation in X-direction at Y = π (centerline of domain) for 45˚ angle of incidence

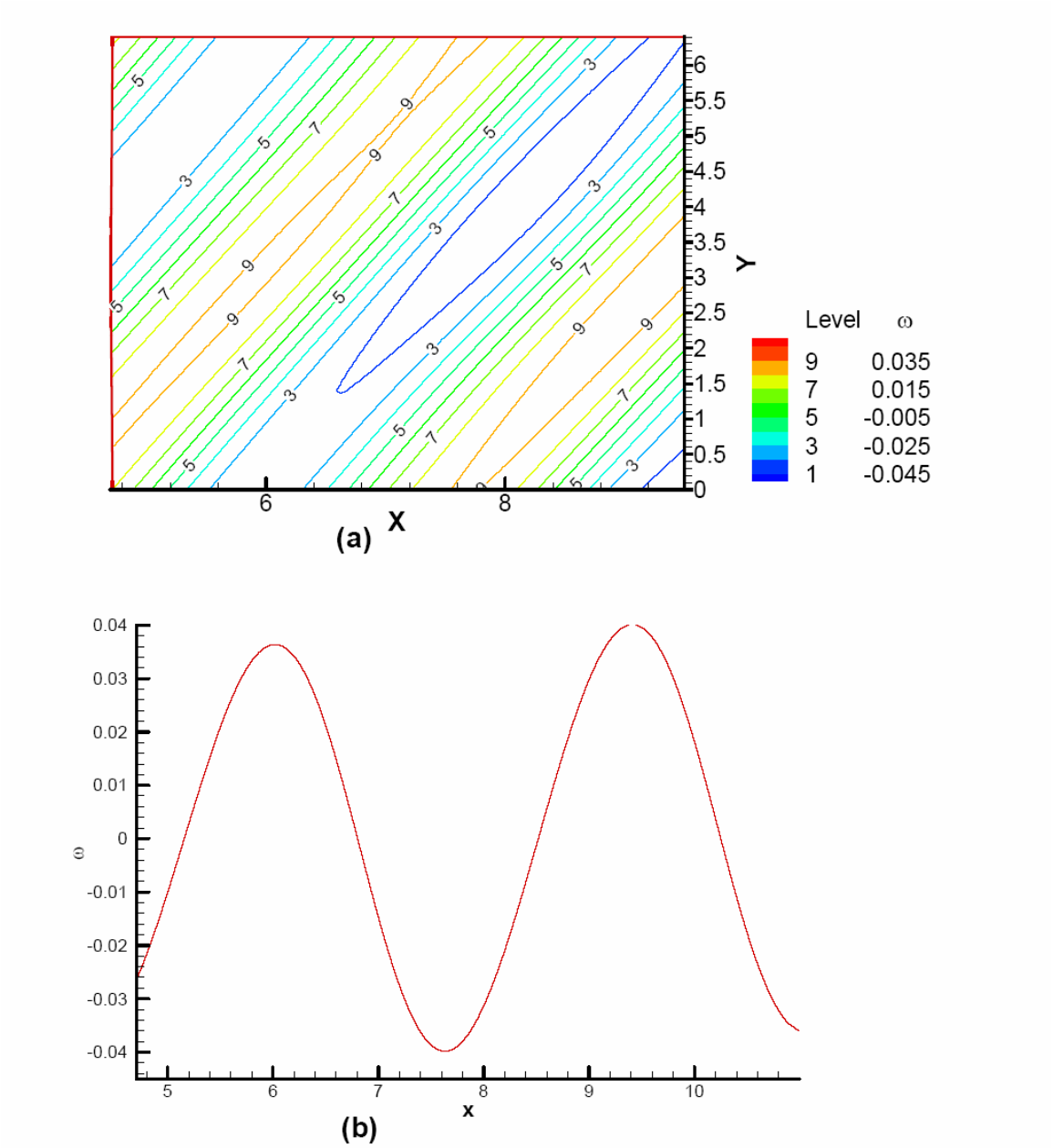

Fig. 13: Interaction of a vorticity-entropy wave at t = 15.0 after start (a) Contours of vorticity (b) Variation in X-direction at Y = π (centerline of domain) for 45˚ angle of incidence.

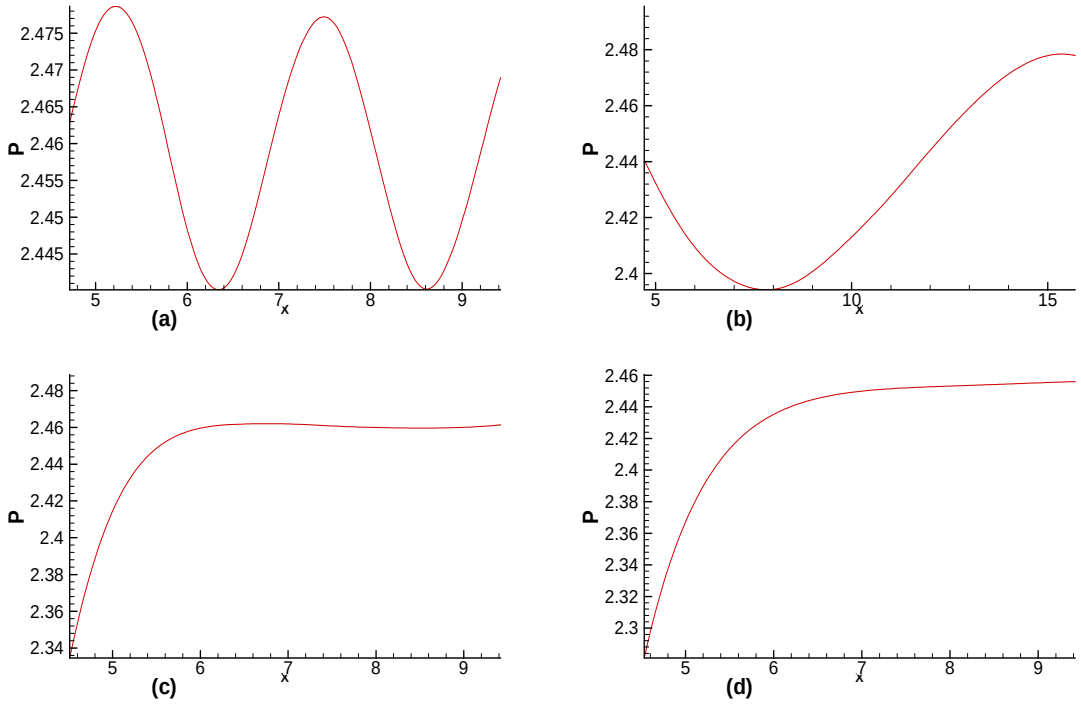

Fig. 14: Pressure profiles in X-direction along Y=π for disturbances coming at angle of inclination of (a) 15˚ (b) 45˚ (c) 75˚ (d) 85˚ with X-axis.

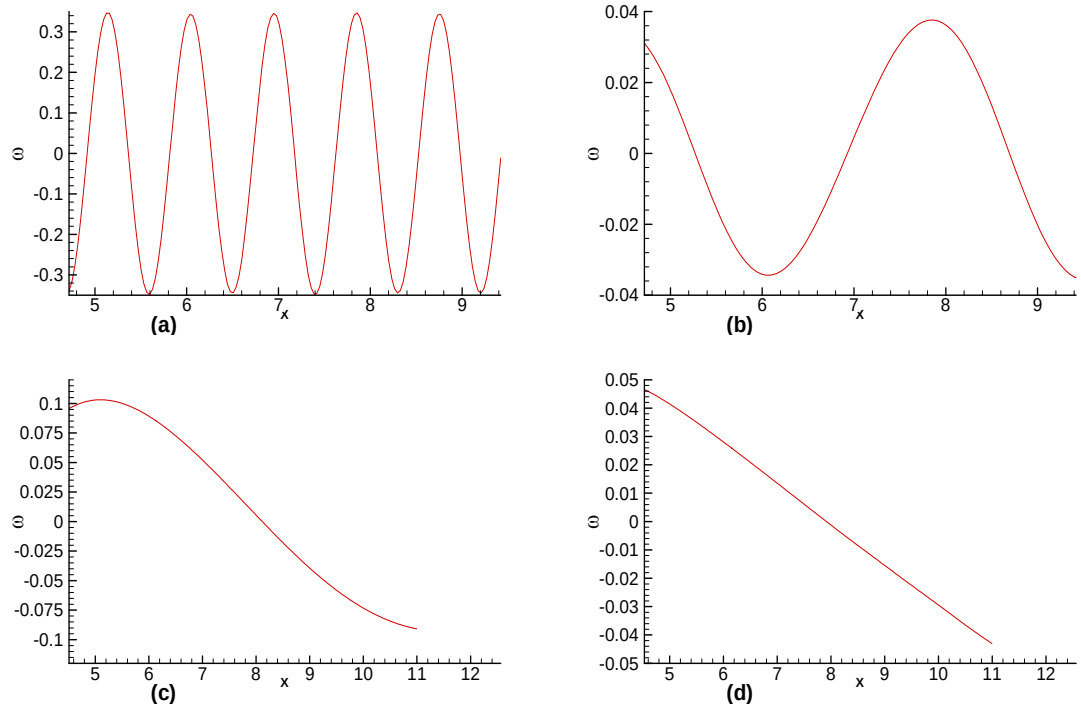

Fig. 15: Vorticity profiles in X-direction along Y=π for disturbances coming at angle of inclination of (a) 15˚ (b) 45˚ (c) 75˚ (d) 85˚ with X-axis.

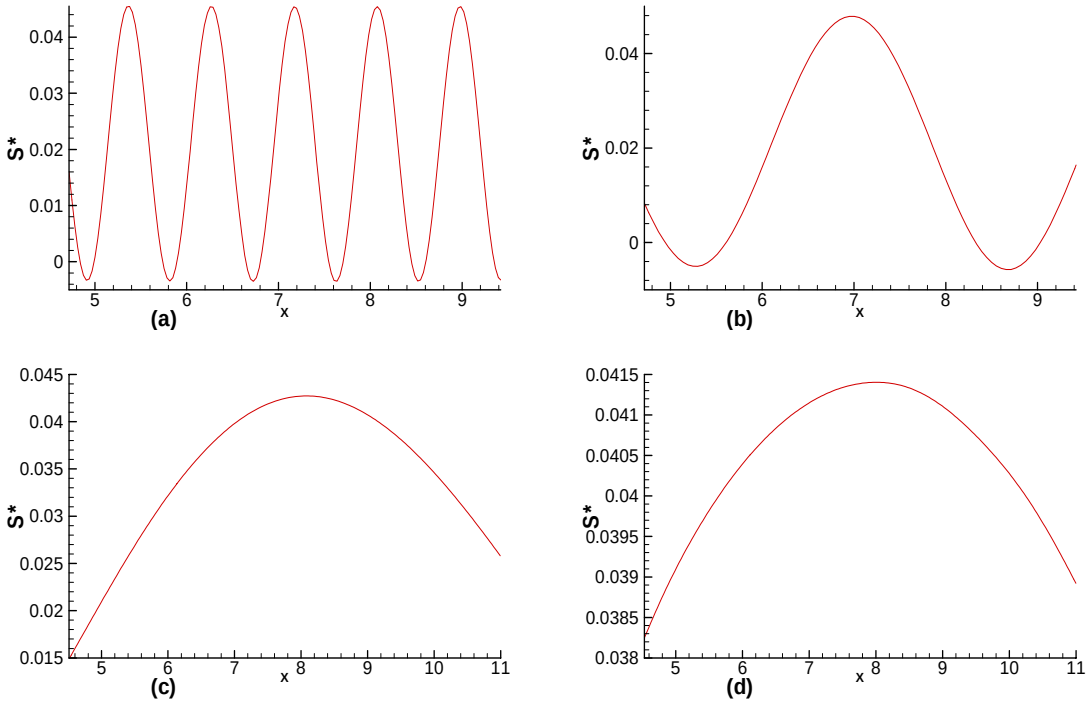

Fig. 16: Profiles of entropy $S^* = \triangle s / C_p$ in X-direction along Y=π for disturbances coming at angle of inclination of (a) 15˚ (b) 45˚ (c) 75˚ (d) 85˚ with X-axis.

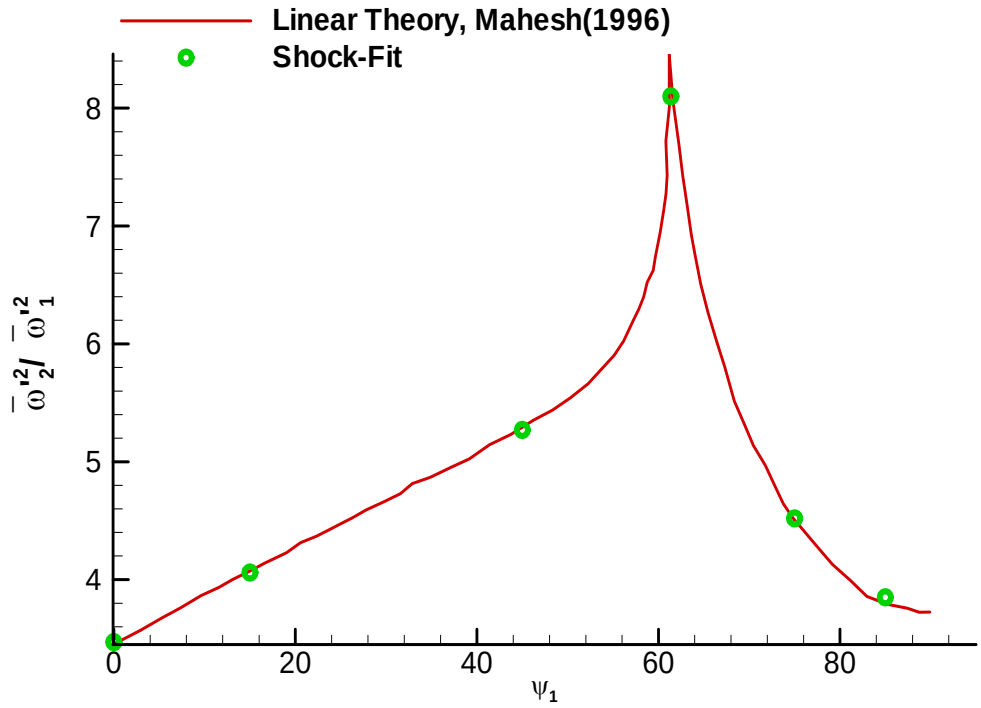

Fig. 17: Comparison between theoretical results (solid) and computational results (dots) from shock-fitting algorithm.

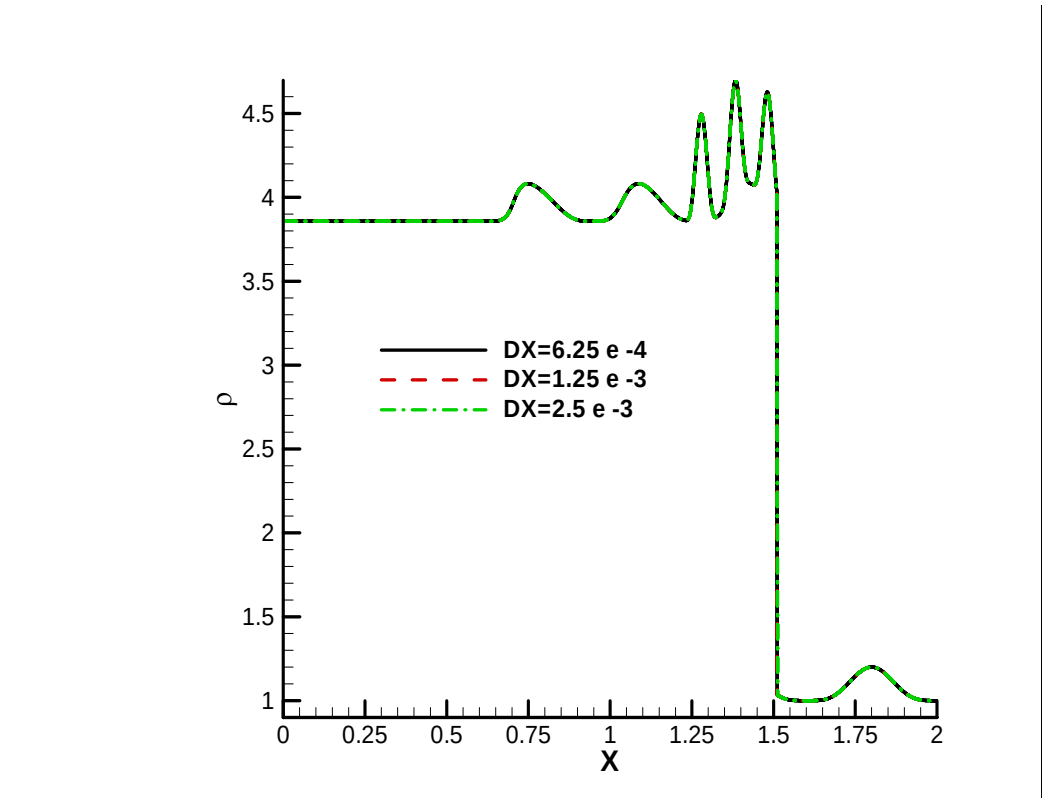

(a)

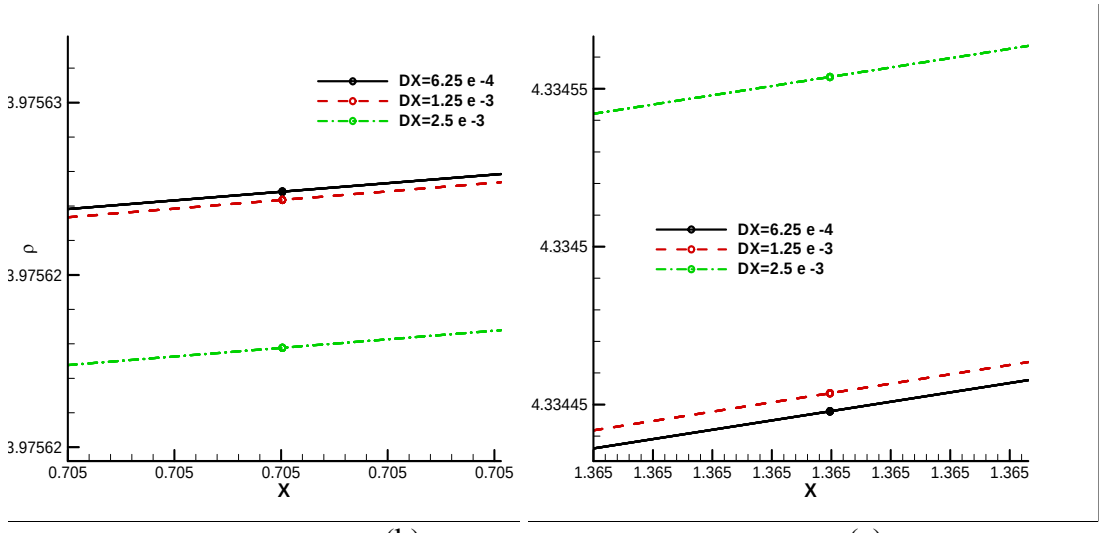

(b) (c)

Fig. 18: (a) Density variation for the smoother version of the Shu-Osher problem for different grid sets. (b) and (c) are zoomed versions of the profile showing convergence.

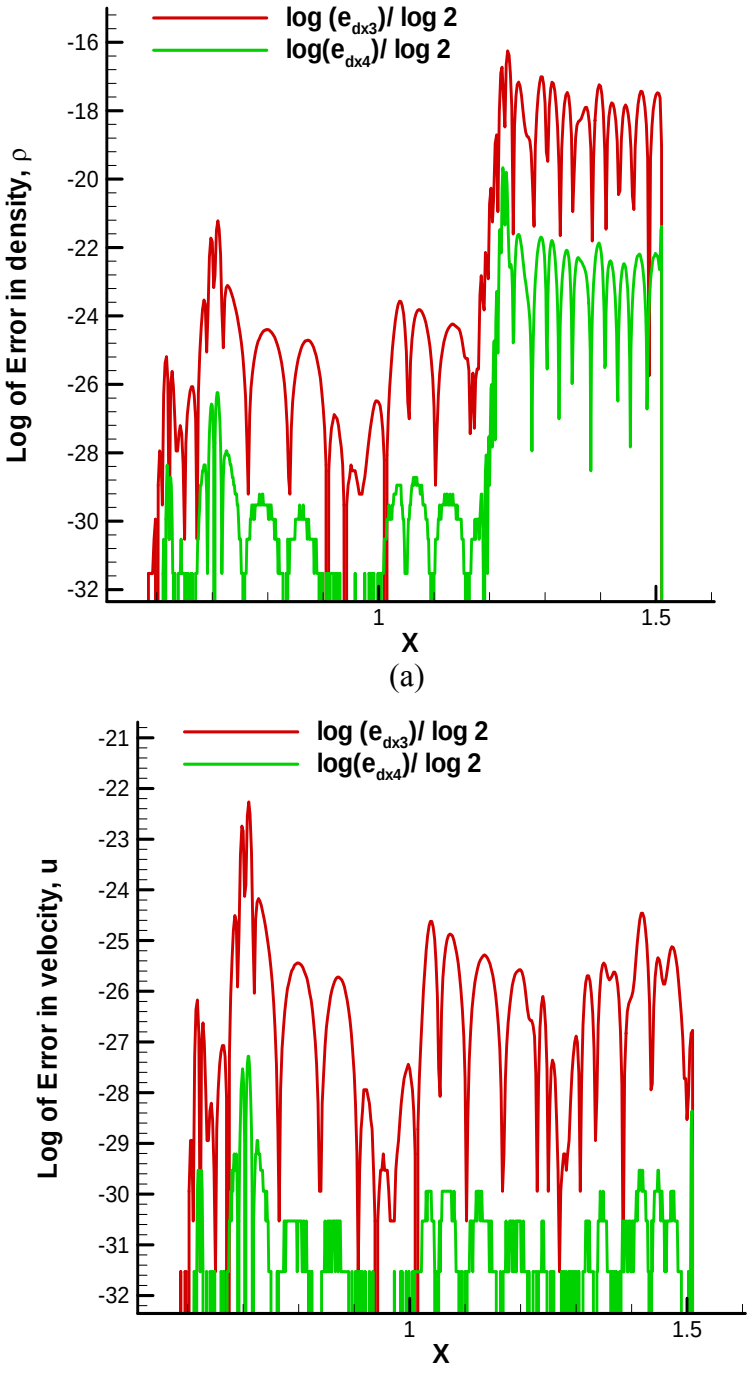

Fig. 19: Comparison of point-wise errors, e_{dx3} and e_{dx4} (defined in Eqs. (32) and (34)) for (a) density and (b) velocity obtained from the front tracking based fixed grid shock-fitting scheme for modified Shu-Osher problem of Suresh [50].

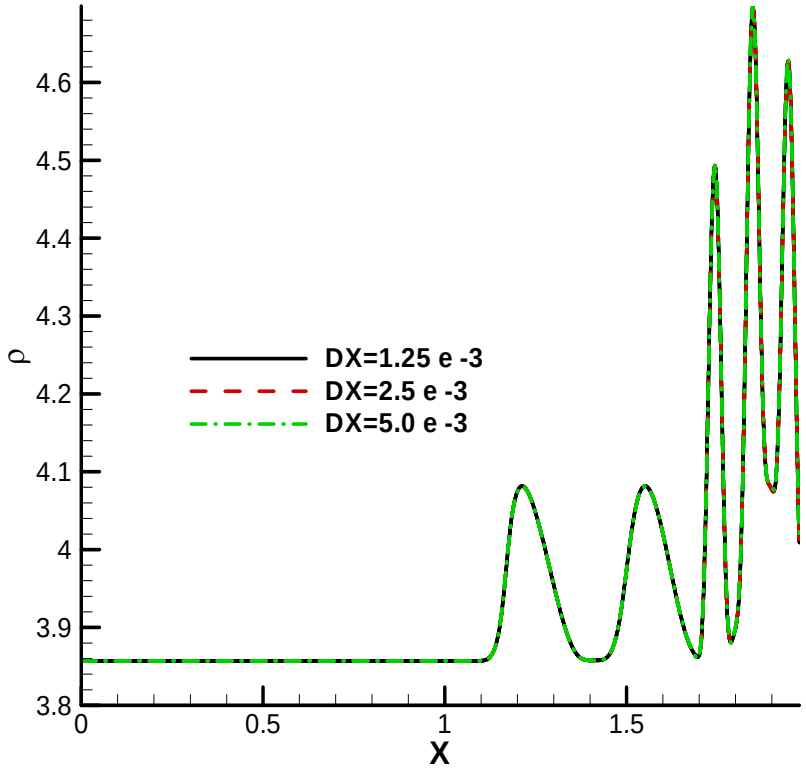

(a)

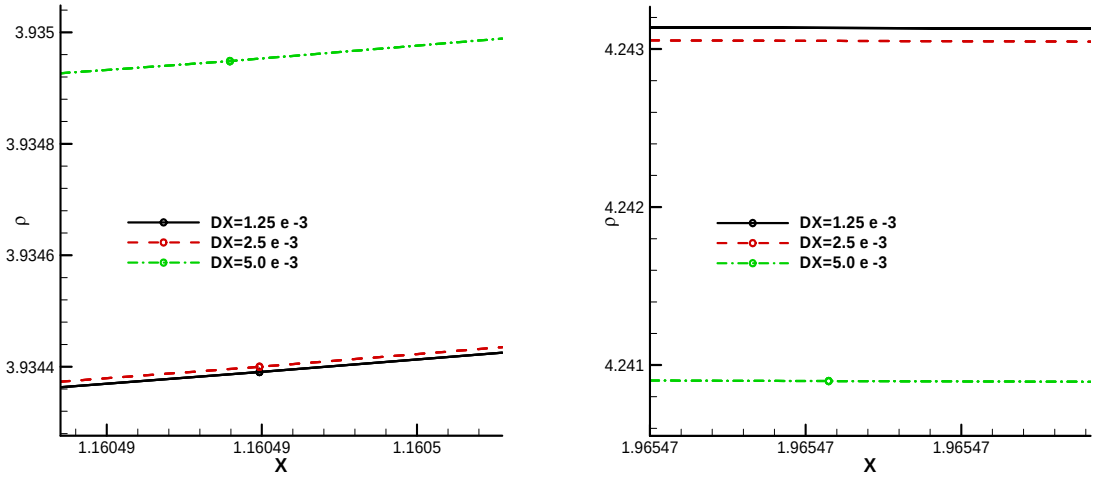

(b) (c)

Fig. 20: (a) Density variation for the smoother version of the Shu-Osher problem obtained from shock-fitting algorithm for different grid sets. Zoomed views of the density profiles are shown (b) away from the shock and (c) near the shock which forms boundary of the domain.

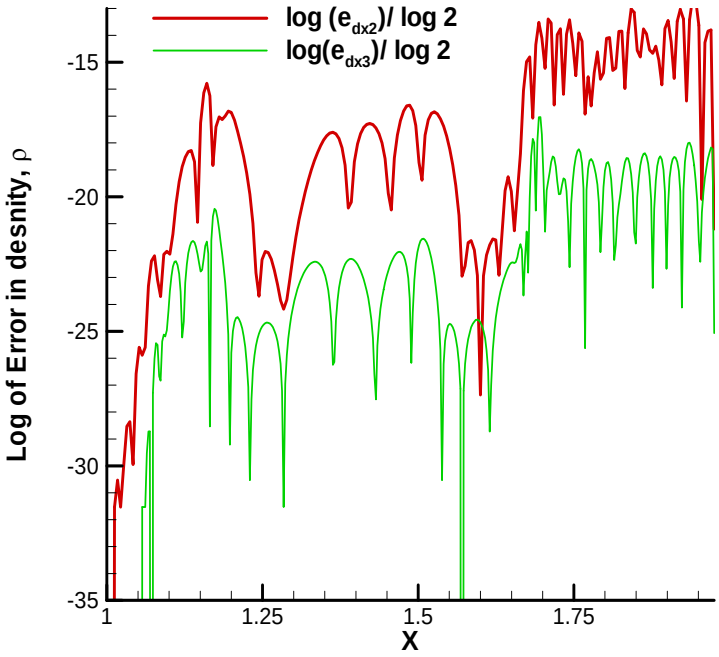

(a)

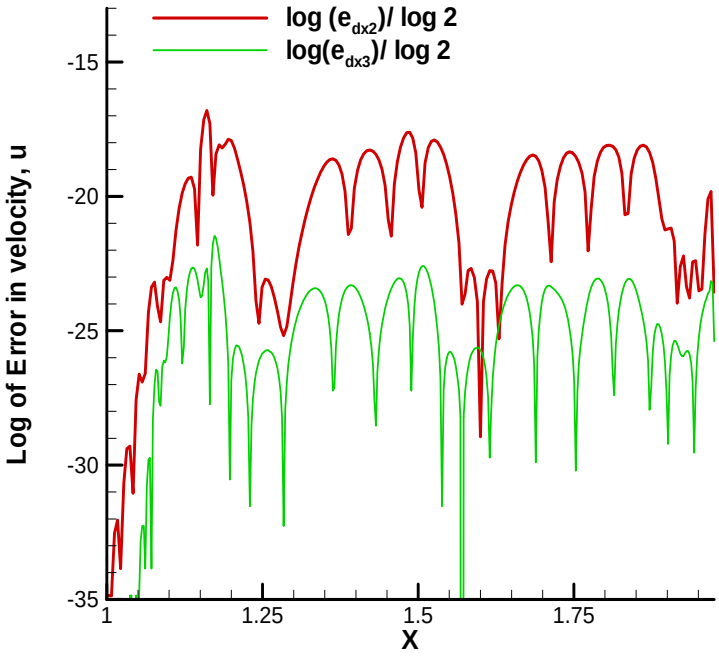

(b)

Fig. 21: Comparison of point-wise errors, e_{dx3} and e_{dx4} (defined in Eqs. (32) and (34)) for (a) density and (b) velocity obtained from the front tracking based fixed grid shock-fitting scheme for modified Shu-Osher problem of Suresh [50].